WIDE BANDWIDTH CONTROL OF HIGH-SPEED MILLING MACHINE FEED DRIVES

By

DAVID ALAN SMITH

A DISSERTATION PRESENTED TO THE GRADUATE SCHOOL
OF THE UNIVERSITY OF FLORIDA IN PARTIAL FULFILLMENT
OF THE REQUIREMENTS FOR THE DEGREE OF
DOCTOR OF PHILOSOPHY

UNIVERSITY OF FLORIDA

1999

ACKNOWLEDGMENTS

The author would like to express his appreciation to his advisor, Dr. Jiri Tlusty, for the opportunity to work on interesting and educationally satisfying research projects during the course of his graduate study. The knowledge and experience that the author has gained under Dr. Tlusty's guidance can only be acquired through years of close work with an exceptionally competent and practical mentor. Special thanks are also extended to members of the author's supervisory committee for their time, assistance, and support toward this work.

The author is most grateful for all of the wonderful friendships he has established with the graduate students in the Machine Tool Research Center. There have been too many to list during the author's extended graduate studies, but each has had a positive influence on the author's professional and personal life.

Finally, the author gives thanks his wife, Donna, for teaching him about the most important things in life.

TABLE OF CONTENTS

page

ACKNOWLEDGMENTS ii

ABSTRACT v

CHAPTERS

1 INTRODUCTION 1

The Goal of High Metal Removal Rate 1
High-Speed Milling 2
The Need for High-Performance Feed Drives in High-Speed Milling 3

2 REVIEW OF LITERATURE 9

3 MODELING OF AXIS FEED DRIVES FOR MACHINE TOOLS 13

Axis Feed Drives for Numerically Controlled Machine Tools 13
Performance of Ballscrew and Linear Motor Feed Drives 16
Feed Drive Control Design for High-Speed Milling 32

4 WIDE BANDWIDTH AXIS MOTION COMMANDS 45

5 WIDE BANDWIDTH CONTROL OF CONVENTIONAL BALLSCREW FEED DRIVES 55

Measured Structural Dynamics on a Ballscrew Feed Drive 55
Design of Wide Bandwidth Axis Control for Ballscrew Feed Drives 57

6 CONTROL OF YAW ERROR ON FEED DRIVES WITH MULTIPLE, NONCOLINEAR MOTORS 76

Yaw Error Reduction Through Coupled Servomotor Control 90
Design of the Yaw Error Control System 95
Simulated Motion Response of the Yaw Regulating Position Control System 108

7 DELAY EQUALIZATION FOR MULTIPLE AXES 113

Comparison of Tracking Errors for Unequal Bandwidth Axes 115
Feedforward Correction of Tracking Errors 116
Frequency Response Comparison for Axes with Different Bandwidths 119
Phase Linearization 126

8 CONCLUSIONS AND RECOMMENDATIONS 135

APPENDICES

A FINITE ELEMENT MODEL OF BALLSCREW FEED DRIVE 139

B YAW ERROR CONTROL SYSTEM PROGRAMS 146

C ALLPASS PHASE EQUALIZATION PROGRAMS 159

REFERENCES 163

BIOGRAPHICAL SKETCH 165

Abstract of Dissertation Presented to the Graduate School
of the University of Florida in Partial Fulfillment of the
Requirements for the Degree of Doctor of Philosophy

WIDE BANDWIDTH CONTROL OF
HIGH-SPEED MILLING MACHINE FEED DRIVES

By

David Alan Smith

August 1999

Chairman: Jiri Tlusty
Major Department: Mechanical Engineering

To fully realize the performance potential of high-speed milling it is necessary to design high-performance axis feed drives for use on high-speed milling machines. It is shown that a 40,000 rpm spindle demands an axis feed drive that is capable of providing 40 m/min feedrates, 20 m/s^2 peak accelerations with a 100 Hz servomotor control bandwidth to effectively utilize high cutting speeds when machining typical aerospace parts. These specifications significantly exceed the axis motion capabilities of conventional machine tools. Achieving this level of performance presents special design challenges for the feed drive components and for the axis control system. Solutions to some of the problems confronting the control system design for wide bandwidth feed drives are presented.

Wide bandwidth, machine tool axes often require special control system compensation to maintain stability in the presence of structural vibration modes that are

inherent in the feed drive system. A control system design is presented that provides a 100 Hz position loop control bandwidth using a conventional ballscrew feed drive. The control system compensation provides stabilization for two torsional, vibration modes that are associated with the ballscrew transmission.

The large accelerations required for efficient, high-speed milling often cause undesirable axis rotation errors. This is especially true for compounded machine axes where the mass center of one axis changes with the position of the other axis or axes. A control system model that simultaneously controls the axis position and the yaw error for an axis with two, linear motors is presented. The control system model demonstrates a 45 times reduction in the yaw error for position commands requiring 10 m/s^2 average acceleration.

High-speed milling machines may not always require wide bandwidth position loop control on all of the machine axes. However, a machine with mismatched axis gains will suffer from excessive tracking error when executing multiple axis motions. A feedforward compensation that provides time delay equalization for the machine axes can reduce tracking errors by two orders of magnitude, for feed drives with a bandwidth ratio of 4:1, without extending the bandwidth of the axes.

CHAPTER 1
INTRODUCTION

The metal cutting process of milling is an important manufacturing process in industrialized nations. Metal parts that are used in everything from consumer goods to military hardware are routinely manufactured by milling operations to tolerances of 10 μm to 250 μm. Milling is used extensively in the automotive industry for the manufacture of engine and drive train components and for the manufacture of sheet metal stamping dies for automobile body panels. Some of the most impressive milling applications can be found in the aerospace industries where large, lightweight structures are milled from solid blocks of aluminum and to a lesser extent from titanium and magnesium. It is common practice to remove as much as 95 percent of the original material by milling to obtain a finished aircraft part. Clearly, enormous amounts of metal must be milled to build a modern aircraft.

The Goal of High Metal Removal Rate

An important specification for a milling operation is the metal removal rate (MRR) which is defined as the volume of metal cut from the part per unit of time. A common goal in milling applications is to maximize this parameter since this will minimize the time required to machine a part. The MRR for a milling process is limited by many factors associated with the machine performance and with the tool life.

Tool life limitations for a given tool material, tool geometry, and part material place limitations on the thickness of the chip cut by each edge of the tool and may also limit the velocity of the tool cutting edge. It is desirable to maximize both of these parameters since they determine how rapidly the tool can advance through the part; however, exceeding these limits leads to substantially shortened tool life.

The machine tool will also have performance limitations which can limit the MRR. The milling spindle has restrictions on speed, power, and torque which may limit the feedrate or the immersion of the tool. The MRR may also be limited by the dynamics of the machine, spindle, and tool structure which can self-excite into chatter vibrations if the tool immersion is excessive [1]. Finally, the maximum velocity and peak acceleration of the machine tool axes must be capable of providing the average feedrate necessary for a given MRR.

High-Speed Milling

The process of milling aluminum using tungsten carbide cutting tools does not present any practical limitation on the cutting edge velocity with regard to tool life [2]. Therefore, it is possible to mill aluminum parts at spindle speeds which are limited only by the capabilities of the machine tool and spindle. This is fortunate, since the MRR is proportional to the spindle speed for constant chip thickness and immersion parameters. Milling with high cutting edge velocity is termed "high-speed milling" and is generally accepted as milling at spindle speeds which exceed 10,000 rpm. Currently, the practical spindle speed limitation for high-speed milling spindles is approximately 40,000 rpm.

The use of high-speed milling in the aerospace industry has become the preferred technology for the manufacture of many aluminum parts, although most parts are still

manufactured on existing conventional low-speed milling machines. According to a U.S. General Accounting Office report [3], high-speed milling technology is responsible for lowering the cost of manufacturing for the McDonnell Douglas F/A-18E/F Strike Fighter. Additionally, many aircraft parts that were formerly made from multiple sheet metal components are now being manufactured more economically from a single block of aluminum by high-speed milling [4]. The quality of the monolithic milled part is also found to be superior when compared with equivalent sheet metal parts assembled with fasteners.

The Need for High-Performance Feed Drives in High-Speed Milling

The use of machine tool spindles with up to 40,000 rpm spindle speed for milling requires the support of high-performance feed drives to achieve improved metal removal rates. This is particularly true for parts which require small repetitive motions, such as aircraft components. For example, when milling aluminum using a 40,000 rpm spindle with a four-fluted tool that is cutting with a 0.25 mm chip load, the required feedrate is 40 m/min. High feedrates, such as these, demand correspondingly large accelerations, as explained by Tlusty et al. [2].

The importance of large acceleration in high-speed milling is illustrated in Figure 1-1 for a 100 mm motion which is typical of pocketing operations in the manufacture of aircraft components. Case A considers the 100 mm path under a 0.2 g ($g = 9.81\ m/s^2$) constant acceleration to a maximum feedrate of 25 m/min followed by a 0.2 g constant deceleration to rest. The total time required to complete the motion is 452 ms, of which, only 28 ms is spent at the desired feedrate of 25 m/min. During the

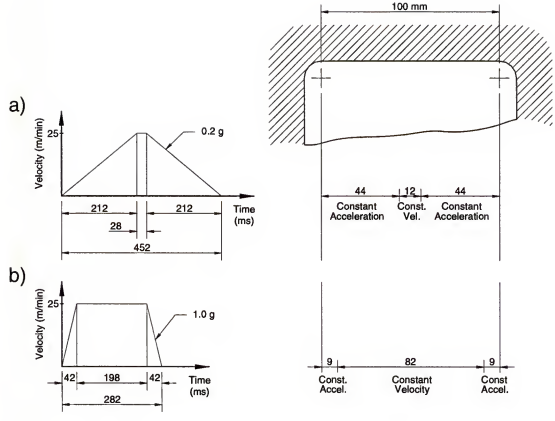

Figure 1-1. Comparison of a typical pocket motion under two different acceleration commands.
a) 0.2 g acceleration; b) 1.0 g acceleration.

acceleration phase, from the start of the motion to the desired feedrate of 25 m/min, the axis traverses 44 mm. Considering the acceleration and deceleration portions of the command, at 0.2 g, the target feedrate of 25 m/min will only be reached for axis movements which exceed 88 mm in length. In case B, the acceleration is increased to 1.0 g and the total time required to traverse the 100 mm motion is now significantly reduced to 282 ms.

In order to accurately track feed drive commands with 1 g and larger accelerations, it is necessary to have a position loop control bandwidth that is at least 100 Hz. This significantly exceeds the typical position loop bandwidth of 10 Hz to 25 Hz, that would be found on conventional low-speed machine tools. This means that the benefits of high-speed milling cannot be achieved by simply attaching a high-speed spindle to a conventional milling machine.

A five-axis, high-speed milling machine (HSMM), which meets the performance demands for high-speed milling, has been designed and built in the Machine Tool Research Center (MTRC) at the University of Florida. A drawing of this machine is shown in Figure 1-2. The table on the machine is mounted vertically, rather than horizontally, to aid in evacuating the machined chips. The vertical table for the machine is carried by compounded axes which are driven by rotary servomotors with ballscrew transmissions. The table is positioned vertically on a cross slide by a single motor to provide the Y axis motion. The cross slide saddle is positioned horizontally by two rotary motors and ballscrews to provide the X axis motion. The compounded X and Y axes are capable of 30 m/min feedrates and 2 g accelerations with a 100 Hz position loop bandwidth. The spindle is carried on a cross slide by a pair of linear motors with similar

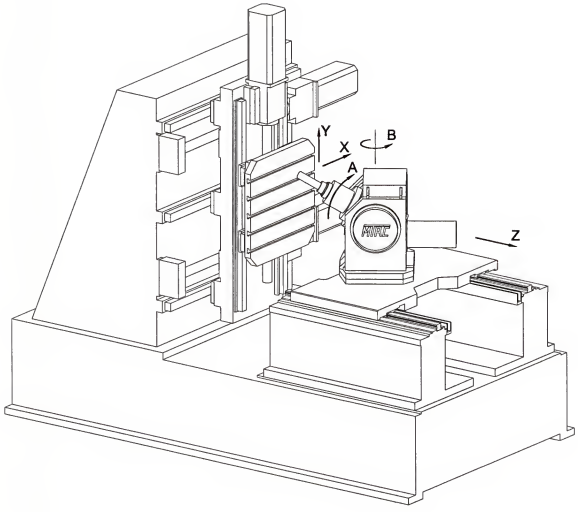

Figure 1-2. Five-axis high-speed milling machine at the Machine Tool Research Center.

performance as the X and Y axes, except the peak acceleration is limited to approximately 0.5 g. The two rotational axes of the machine are currently under completion.

The MTRC machine has served as the basis for all modeling and as the test bed for all control system implementations that will be discussed in this dissertation. It has been used to manufacture numerous aluminum parts which are typical of the monolithic components used in modern aircraft applications. The aluminum part shown in Figure 1-3 was manufactured on the machine. This part is representative of the challenges confronting modern aircraft component manufacturing. The hexagonal walls on the part are 95 mm high and are only 0.5 mm thick. The part is machined from a solid 8.5 kg aluminum block. The finished part is reduced to only 1.5 percent of the original mass (128 g) during 28 minutes of high-speed machining at a spindle speed of 28,500 rpm.

The purpose of this dissertation is to investigate some of the problems that are confronted in wide bandwidth control of feed drives for high-speed milling machines. This work presents methods of coping with these problems, and in some cases, these solutions have been implemented on the MTRC high-speed milling machine. The results presented in this dissertation demonstrate that the performance demands that high-speed milling places on the servomotor control system can be satisfied by using specialized control strategies along with modern control system hardware.

Figure 1-3. Sample monolithic aluminum part manufactured on the MTRC five-axis high-speed milling machine.

CHAPTER 2
REVIEW OF LITERATURE

There has been much research on control strategies for machine tool servo drives in the past two decades. The introduction of the digital signal processor (DSP) for servomotor control has allowed advanced control algorithms to be executed with fast servomotor loop closing times. Most of these studies have concentrated on feedback and feedforward compensation techniques to achieve minimal tracking error performance. An excellent summary of the control systems research is given by Koren [5].

Several researchers have applied modern and robust control design strategies for the purpose of tolerating uncertainties in the plant model. The H infinity (H_∞) design procedure was applied by Alter [6] to obtain 46 percent greater stiffness in the presence of parameter uncertainties. Van Brussel [7] applied H_∞ and sliding mode control to linear motors with a varying table mass as a parameter uncertainty. He found that mass changes of up to 300 percent could be accommodated with acceptable tracking error.

There is one approach that attempts to couple the control of all axes to minimize the contour error. A cross-coupling controller has been proposed by Koren [8] to include feedback from all axes to generate the correction signals for each axis based on the contour error.

The feedforward approach, to control system compensation, consists of prefiltering the command in a manner that compensates for the distortions that the position

loop system will impose on an axis command signal. The common approach is to invert a transfer function model of the position loop to use as a feedforward system. The cascaded sequence of the feedforward system and the position loop control system results in an overall transfer function of unity. In theory, the servomotor will then execute any command without error. An important work based on this approach is the zero phase error tracking control (ZPETC) proposed by Tomizuka [9]. The method uses an inverse system model with a zero phase error compensation for position loop zeros that would lead to unstable feedforward poles. The simulated results of this approach show excellent tracking error performance, but the author points out that the performance is sensitive to modeling errors and plant variations. Tomizuka, also, developed an adaptive version of the ZPETC [10], which was effective at cancelling slowly changing plant dynamics. One limitation of the ZPETC method is that the amplifier may reach a saturation limit if the command is too harsh such as in a corner motion. A solution proposed by Weck [11] is to include a lowpass filter with the feedforward system to remove the high frequency components from the command. This can prevent saturation and give a better tracking performance under certain types of commands.

Most researchers have only considered the position response of the axis to a position command signal. However, there is also a need to obtain a high dynamic stiffness at the workpiece with respect to the cutting force input at this point. This response is important for stability against regenerative chatter. Chen and Tlusty [12] simulated the control of wide bandwidth servomotor feed drives with a single, lightly damped mode in a ballscrew drive. They considered the positioning performance and the disturbance force rejection for three servodrive systems in their work, as shown in Figure 2-1. The first

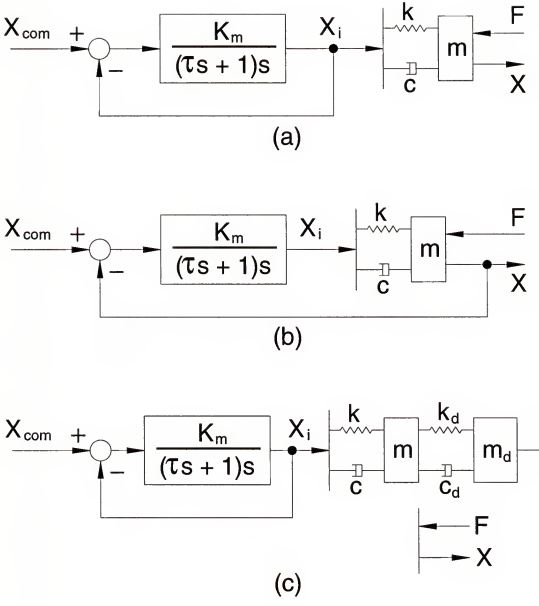

Figure 2-1. Three wide bandwidth servodrive configurations studied by Chen and Tlusty.
a) Feedback from a rotary encoder; b) Feedback from a linear encoder;
c) Feedback from a rotary encoder with a passive damper.

arrangement consisted of feedforward compensation for a system with feedback from a rotary encoder with the flexible mode outside of the control loop, as shown in Figure 2-1a. The second configuration used feedback from the table with a linear encoder, as shown in Figure 2-1b. This configuration also used feedforward compensation to improve position accuracy. The control system utilized accelerometric feedback to stabilize the position loop in this configuration. The third system used a passive, tuned damper to modify the dynamics of the drive system with feedback from a rotary encoder, as shown in Figure 2-1c.

With the exception of the work by Chen and Tlusty, the work to date has focused primarily on conventional low-speed machine tool servomotor control with performance, that is typically, limited to peak accelerations below 0.2 g and position loop control bandwidths that are less than 25 Hz. In these applications, the servomotor and feed drive assembly can be adequately modeled as a second order system. As the position loop control bandwidth is increased, it becomes necessary to contend with the structural dynamics of the feed drive. This leads to higher order plant models with more challenging control system compensation. The goal of the research presented in this dissertation is to develop feedback control systems that effectively deal with the structural dynamics of the feed drive system to achieve the wide bandwidth position control required for high-speed milling.

CHAPTER 3
MODELING OF AXIS FEED DRIVES FOR MACHINE TOOLS

Machine tool feed drives for high-speed milling applications require wide bandwidth performance. Fast axis response is required for executing the rapidly changing motion commands as well rejecting disturbance forces that attempt to drive the axis out of the commanded position. The most important disturbance force is assumed to be the cutting force. This force depends on the geometry of the motion program and is therefore, an unknown disturbance for the position loop control system.

In conventional bandwidth axis control systems, the drive structure is typically modeled as a rigid body with an inertia that resists acceleration under the applied motor torque or force. By comparison, wide bandwidth feed drives often require higher order dynamic models for the drive structure, in order to successfully design the control system for stability.

Axis Feed Drives for Numerically Controlled Machine Tools

Modern machine tools use, primarily, two different types of axis feed drive designs for linear motion. The two designs, for an axis that drives the machine table, are shown in Figure 3-1. The design shown in Figure 3-1a, uses a ballscrew and a recirculating ballnut to transmit linear motion to the table from a rotary servomotor. The table is supported by roller guideways, that constrain the table to provide linear motion in only one direction. This axis drive design has been the conventional configuration for

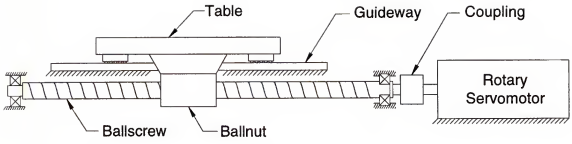

(a)

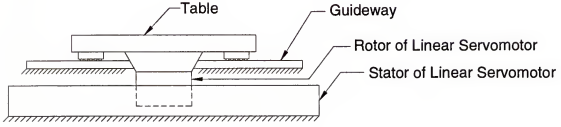

(b)

Figure 3-1. Comparison of two machine tool axis feed drives.
a) Conventional, ballscrew axis feed drive; b) Modern, linear motor axis feed drive.

providing linear motion on numerically controlled machine tools. In this design, the feedback of the axis position can be taken indirectly from the angular position of the servomotor rotor, or it may be measured directly from the actual position of the axis using a linear position sensor. This conventional drive design has the advantage of providing good positioning accuracy at a reasonable cost for many applications. This drive design also has the benefit of establishing mechanical isolation between the servomotor and the table.

The most common motor type for machine tool position control applications is the DC servomotor. There are two basic constructions for this type of motor. The traditional design uses the commutator and carbon brush construction. This motor type is still commonly used for machine tool servomotors. The modern brushless DC servomotor design eliminates the commutator and brushes, that require periodic maintenance, but requires additional control complexity to electronically perform the commutation operation. Iron core brushless DC motors also suffer from a small cogging torque disturbance, that can result in small position errors during motion. Both types of DC servomotors are preferred over other motor designs because of their relatively small rotor inertia and for their ability to develop a large peak torque, that is proportional to the applied armature current, regardless of rotor speed.

A more modern axis feed drive design is shown in Figure 3-1b. This design uses linear motor technology to directly drive the table, without the need for a mechanical transmission to convert from rotary motion to linear motion. The linear motor construction can be viewed as a rotary motor which is cut radially to the rotor centerline and, then, unrolled to lie flat. This is not how a linear motor is manufactured, but it gives an

understanding of how these motors function. Linear motors can be made based on several different principals of operation, which are analogous to rotary motor designs. Like the DC rotary servomotor, the DC linear servomotor is the design of choice for machine tools due to its small rotor mass and its ability to develop large forces at all motor speeds.

The linear motor feed drive system is currently gaining acceptance for high-performance machine tools, although, the conventional ballscrew design is still the most prevalent for machine tool feed drives. The axis position on a linear motor drive is always read directly using a linear position sensor. The linear motor feed drive is considerably easier to design and install than the conventional ballscrew feed drive, and it offers improved performance for certain parameters. The drawbacks are that the overall cost of a linear motor axis is substantially higher and that some performance measures are potentially reduced. Deciding which design to use in a machine tool application is not a simple task. Each drive type has important advantages, which must be weighed against the performance demands placed on the axis. Table 3-1 lists some of the common advantages and disadvantages of both axis drive types.

While the axis drive designs shown in Figure 3-1 are currently the most common, there are other designs which are often used in machine tool feed drives. For example, when extremely long axis travels are required, it is common to use an antibacklash rack and pinion drive design. In this chapter, however, only the ballscrew and the linear motor feed drives will be considered as candidates for high-speed milling applications.

Performance of Ballscrew and Linear Motor Feed Drives

The performance of ballscrew and linear motor feed drives can differ substantially, even when the position loops are tuned for the same nominal response. To illustrate the

Table 3-1. Comparison of ballscrew and linear motor axis feed drives.

	Advantages	Disadvantages
Ballscrew Feed Drive	• Economical • Insensitive to changes in axis inertia • Reduced sensitivity to axis disturbance forces under certain conditions	• Limited control bandwidth over long travel distances • Speed and acceleration limited • Backlash and friction nonlinearities • Limited life under high accelerations and high feedrates
Linear Motor Feed Drive	• Wide bandwidth control over an unlimited travel distance • High speed and acceleration • Minimal backlash and friction • Simple design and installation • Long life • Fewer components	• Expensive • Sensitive to changes in axis inertia • Sensitive to axis disturbance loads

differences between these two axis drive technologies, dynamic models of the feed drive control systems will be developed. The models will be used to investigate the robustness against changes in the axis mass and to evaluate the ability to reject external disturbance forces applied to the axis. When necessary, numerical values for component parameters will be taken from the Y axis design on the MTRC high-speed milling machine to draw conclusions.

In the manufacture of aluminum aircraft components, it is common for the mass of the workpiece to change substantially during the milling process. The change in the workpiece mass represents a time-varying change in the servomotor system for the machine axes that move the table. If the axis inertia is sensitive to changes in the

workpiece mass, then the transient servomotor performance may be degraded to an unacceptable level when a wide range of workpiece masses are attached to the table.

The cutting forces produced during milling tend to drive the axis out of the desired position. This is undesirable because it produces dimensional errors in the finished part. Therefore, it is essential that the position loop be stiff against displacements resulting from the cutting process, or any other loads, which might lead to machining tolerance errors. The cutting forces in milling vary proportionally with the axis feedrates when the spindle speed is held constant. Since the axis feedrates change rapidly in high-speed milling, the position loop must have a high axis stiffness over the entire control bandwidth. It would not be sufficient to achieve high stiffness only at low frequencies, as could easily be obtained by using an integral control gain within the position control loop.

A simplified block diagram of the position loop for the Y axis on the MTRC high-speed milling machine is shown in Figure 3-2. This axis uses a conventional ballscrew feed drive transmission to achieve performance suitable for high-speed milling applications. The control model shown in Figure 3-2 represents the most fundamental form of a positional servomotor with position feedback taken from the rotor. The inner feedback loop with the proportional gain, K_v, controls the motor velocity, while the outer feedback loop with the proportional gain, K_p, controls the motor position. In this model, the discrete-time portions of the position loop control are approximated as a continuous-time system to simplify the current presentation. More accurate models, based on discrete-time control theory, will be presented in subsequent chapters. This model assumes that the ballscrew is a rigid element when compared to the stiffness of the position loop against

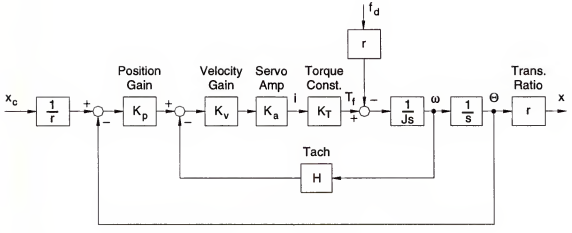

Figure 3-2. Block diagram for the rigid ballscrew position loop model.

displacement at the table. In this rigid ballscrew model, the table position, x, is related to the rotor angle, Θ, by a constant, r, called the ballscrew transmission ratio.

$$x = r\Theta \tag{3-1}$$

On the MTRC high-speed milling machine the ballscrew transmission ratio is 0.00318 m/rad (20 mm/rev).

The servomotor uses a pulse-width modulated, transconductance power amplifier to control the motor armature current. The torque developed in the electromagnetic field, T_f, of the motor is equal to the product of the motor torque constant, K_T, and motor current, i, by

$$T_f = K_T i \tag{3-2}$$

Analysis of this block diagram shows that the position loop response at the table, $X(s)$, due to the position command, $X_c(s)$, and due to the disturbance force, $F_d(s)$, is given by

$$X(s) = \frac{\omega_p^2}{s^2 + 2\zeta_p\omega_p s + \omega_p^2}\left[X_c(s) - \frac{1}{\left(\frac{J}{r^2}\right)\omega_p^2}F_d(s)\right] \tag{3-3}$$

where:

$\omega_p = \sqrt{\frac{K_p K_v K_a K_T H}{J}}$ = Position loop natural frequency

$\zeta_p = \frac{H}{2}\sqrt{\frac{K_v K_a K_T}{J K_p r}}$ = Position loop damping ratio

K_a = Servo amplifier gain

H = Tachogenerator constant

J = Total mass moment of inertia referenced to the rotor

The mass moment if inertia, J, in Equation 3-3, can be expressed in terms of the combined mass moment of inertias for the rotational components and the masses of the table and workpiece as

$$J = J_R + (m_t + m_w)r^2 \tag{3-4}$$

where:

J_R = Mass moment of inertia of rotor, coupling and ballscrew (0.027 kg m^2)

m_t = Table mass (225 kg)

m_w = Workpiece mass

The values for these parameters on the Y axis of the MTRC high-speed milling machine are specified in parentheses.

The position loop bandwidth and damping ratio are shown, in Equation 3-3, to depend on the total mass moment of inertia of the system. Additionally, the system mass moment of inertia is shown, in Equation 3-4, to depend on the mass of the workpiece. Therefore, changes in the workpiece mass will change the position loop performance. However, due to the small value of the ballscrew transmission ratio, r, the workpiece will have a small effect on the mass moment of inertia when referenced to the rotor. For example, consider a part that will be machined from a solid block of aluminum that is 60 cm square and 20 cm thick with a mass of 200 kg. This is approximately the largest size part which could be milled on the MTRC machine yet it would only increase the total mass moment of inertia by 6.9 percent. The ballscrew transmission isolates the table and workpiece inertia from the servomotor control system. Therefore, the performance of the ballscrew feed drive will be robust to variations of the workpiece mass due to the large system inertia inherent in the rotational components of this type of drive.

Equation 3-3 also indicates that the stiffness against disturbance forces applied to the table is essentially constant over the bandwidth of the position loop and is given by

$$k_d = \left(\frac{J}{r^2}\right)\omega_p^2 \tag{3-5}$$

The quantity

$$M_{sys} = \frac{J}{r^2} \tag{3-6}$$

can be interpreted as the mass of the feed drive system referenced to the table. This parameter can be very large for a ballscrew feed drive due to the small ballscrew transmission ratio. On the Y axis of the MTRC machine, it is nearly 2900 kg without considering any workpiece mass. According to this model, the feed drive stiffness will be proportional to the parameter M_{sys} for a given position loop natural frequency ω_p. Considering two different feed drive systems with equal natural frequencies, the system with the larger system mass will have the highest stiffness against disturbance forces.

The drive stiffness is also proportional to the square of the position loop natural frequency. A plot of the drive stiffness versus the position loop bandwidth is shown in Figure 3-3, using the parameters given for the MTRC machine. The axial stiffness of the ballscrew and ballnut drive assembly used on this machine is approximately 50 N/μm. Based on the parameters used to plot Figure 3-3, the stiffness of the position loop exceeds the stiffness of the ballscrew for control bandwidths which are greater than 21 Hz. Therefore, this model is only valid for conventional bandwidth applications where the position loop stiffness is much smaller than the ballscrew stiffness. In high-speed milling applications, it is necessary to have position loop control bandwidths in excess of 50 Hz.

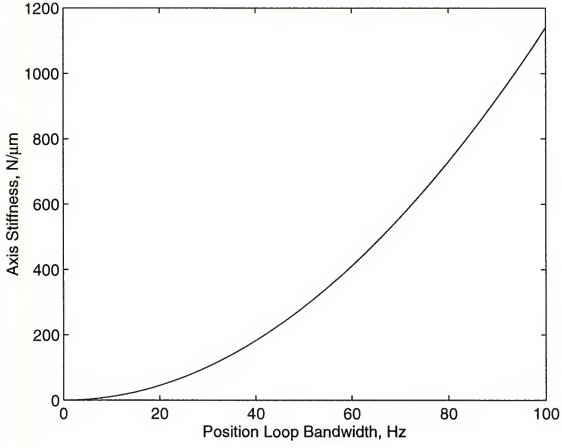

Figure 3-3. Axis stiffness of the MTRC milling machine for a rigid ballscrew feed drive model.

At these bandwidths, the control loop may become much stiffer than the ballscrew transmission, and the modeling assumption of a rigid ballscrew drive is invalid.

To investigate wide bandwidth control of ballscrew feed drives, a different model can be constructed to include the effects of the compliance in the ballscrew and ballnut. In this model, it is assumed that the stiffness that is derived from the position loop is much greater than the axial stiffness of the ballscrew components. In addition, it is assumed that the table and workpiece masses are negligible with respect to the inertia of the rotational components. This allows the servomotor position loop to be separated from the dynamics of the ballscrew and table system when the position feedback is taken from the rotor. The position loop control will therefore position the rotor with the same performance as the rigid ballscrew model; and, it will not be coupled with the dynamics created by the ballscrew and table.

The ballscrew flexibility, combined with the mass of the table and workpiece, creates a single degree-of-freedom system with a vibrational response that is considered external to the position loop. A structural model of the compliant ballscrew feed drive system is shown in Figure 3-4. This single degree-of-freedom model represents a system undergoing base motion from the input position, x_r, and forced response from the disturbance force, f_d. The position x_r is the position the table would be in if the ballscrew were perfectly rigid. The position x is the actual position of the table for the compliant ballscrew model. The theoretical position x_r is equal to the rotor angular position times the ballscrew transmission ratio. The axis position response due to these two inputs can be expressed in the Laplace domain as

$$X(s) = \left(\frac{2\zeta_d\omega_d s + \omega_d^2}{s^2 + 2\zeta_d\omega_d s + \omega_d^2}\right)X_r(s) - \frac{1}{k_d}\left(\frac{\omega_d^2}{s^2 + 2\zeta_d\omega_d s + \omega_d^2}\right)F_d(s) \tag{3-7}$$

where:

$\omega_d = \sqrt{\frac{k_d}{m_t + m_w}}$ = Ballscrew feed drive natural frequency

$\zeta_d = \frac{c_d}{2\sqrt{k_d(m_t + m_w)}}$ = Ballscrew feed drive damping ratio

k_d = Axial stiffness of ballscrew and ballnut

c_d = Axial damping of ballscrew and ballnut

The base motion response of the compliant feed drive system behaves like a mechanical lowpass filter between the input and the output positions. At frequencies well below the natural frequency of the drive, the axis position follows the input, x_r, without significant dynamic errors. At excitation frequencies near resonance, the axis position response may be much greater than the input position. At frequencies above the resonance region, the axis position response rolls off with increasing frequency of the input position. This places practical limitations on the useful operation bandwidth of the drive.

In this model, the disturbance force does not load the servomotor control system. This means that the disturbance force, f_d, affects the axis position but does not influence the rotor position. Therefore, the theoretical axis position x_r depends only on the position loop command input, x_c, and the position loop transfer function given by

$$\frac{X_r(s)}{X_c(s)} = \frac{\omega_p^2}{s^2 + 2\zeta_p\omega_p s + \omega_p^2} \tag{3-8}$$

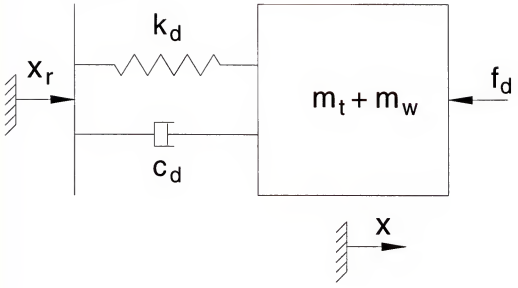

Figure 3-4. Structural model of compliant ballscrew feed drive.

The parameters, ω_p and ζ_p, in Equation 3-8 are the position loop bandwidth and damping ratio, respectively. These quantities determine the servomotor position response at the rotor.

A block diagram of this compliant feed drive model is shown in Figure 3-5. The position loop response, $X(s)$, due to the axis position command, $X_c(s)$, and due to the disturbance force at the table, $F_d(s)$, is now given by

$$X(s) = \left(\frac{\omega_p^2}{s^2 + 2\zeta_p\omega_p s + \omega_p^2}\right)\left(\frac{2\zeta_d\omega_d s + \omega_d^2}{s^2 + 2\zeta_d\omega_d s + \omega_d^2}\right)X_c(s) - \frac{1}{k_d}\left(\frac{\omega_d^2}{s^2 + 2\zeta_d\omega_d s + \omega_d^2}\right)F_d(s) \tag{3-9}$$

The demand for fast servomotor response in high-speed milling may lead to a position loop control bandwidth that is greater than the natural frequency, ω_d, of the axial mode of the ballscrew feed drive system. In this case, the bandwidth of the axis will be approximately limited to the axial mode natural frequency of the ballscrew. In addition, the damping ratio of the ballscrew axial mode is usually very small; therefore, the axis frequency response will be highly resonant. This may lead to position overshoots for the wide bandwidth axis commands that are commonly used in high-speed milling.

It is possible to apply feedforward correction to the axis command, $X_c(s)$, to compensate for the dynamics of the feed drive. However, the natural frequency, ω_d, and damping ratio, ζ_d, depend on the workpiece mass and on the axial stiffness of the ballscrew, which varies with the position of the ballnut along the ballscrew axis. Therefore, any attempt at feedforward compensation must be adaptive to the slow but substantial changes in the dynamics of the feed drive.

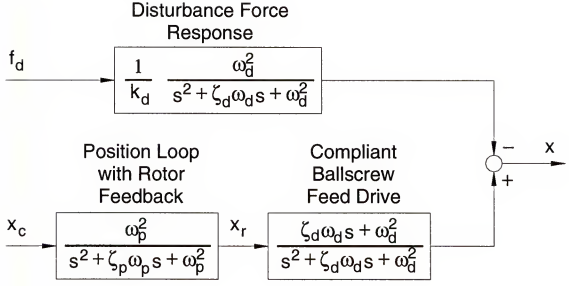

Figure 3-5. Compliant ballscrew position loop block diagram.

In this compliant ballscrew model of the axis feed drive, the servomotor holds the rotor in the commanded position in the presence of disturbance forces. Since the ballscrew flexibility is external to the position control loop, the table position will respond as a lowly damped, second order spring mass system to any disturbance forces that are applied to the axis. The response characteristic, between the disturbance force and the table position, is apparent in Equation 3-9.

It has become common practice to use linear position scales to directly feed back the axis position with ballscrew feed drives. This is usually done for small bandwidth axes, where the intent is to eliminate errors caused by backlash, friction, ballscrew pitch errors and ballscrew thermal growth. With feedback of the axis position, it is also possible to increase the axis stiffness against disturbance forces. When this technique is applied to wide bandwidth axis feed drives, it becomes necessary to apply special control compensation to maintain stability in the position loop [12]. This control compensation must also be robust against the same parameter changes that make feedforward compensation difficult.

A simplified block diagram of a linear motor feed drive is shown in Figure 3-6. As in the previous models, the discrete-time nature of the position loop control has been approximated as a continuous-time system to simplify the analysis, and to allow comparison with the models developed for the ballscrew feed drive axis. The linear motor position loop response, $X(s)$, due to the position command, $X_c(s)$, and due to the disturbance force, $F_d(s)$, at the table is given by

$$X(s) = \frac{\omega_p^2}{s^2 + 2\zeta_p\omega_p s + \omega_p^2}\left[X_c(s) - \frac{1}{(m_t + m_w)\omega_p^2}F_d(s)\right] \tag{3-10}$$

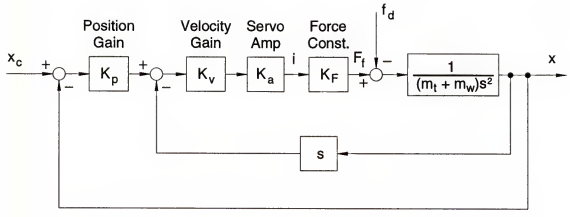

Figure 3-6. Linear motor feed drive position loop block diagram.

If the control bandwidths are equal for the rigid ballscrew feed drive system and for the linear motor system, then the position loop response to commands will be identical for these two feed drives. This can be seen by comparing the ballscrew feed drive response from Equation 3-3 with Equation 3-10. However, the linear motor feed drive may permit a wider position loop control bandwidth than the compliant ballscrew feed drive model. The improvement in performance results from eliminating the ballscrew transmission, which creates a flexible link between the servomotor and the table.

The linear motor feed drive with the control system block diagram shown in Figure 3-6 provides an axis stiffness at the table; that is effectively constant over the full control bandwidth of the position loop. Equation 3-10 indicates that the stiffness against disturbance forces for the linear motor axis is

$$k_d = (m_t + m_w)\omega_p^2 \tag{3-11}$$

The linear motor stiffness is similar to the stiffness parameter for the rigid ballscrew model except that the inertia terms associated with the rotational elements are eliminated in Equation 3-11. The system mass for the MTRC high-speed milling machine with the ballscrew feed drive is $M_{sys} = J/r^2 = 2900$ kg. This is almost thirteen times larger than the mass of $m_t = 225$ kg that is assumed for the linear motor feed drive model. If it is assumed that the position loop control bandwidths are equal and the linear motor rotor and workpiece masses are negligible, then the rigid ballscrew feed drive is about an order of magnitude stiffer than the linear motor axis. This result would only be true for small control bandwidths where the rigid ballscrew model applies. For wide bandwidth position loop control where the compliant ballscrew model is valid, the linear motor may develop the highest stiffness. This is due to the fact that the ballscrew and ballnut limit the feed

drive stiffness for this mode, while the linear motor stiffness increases with the square of the position loop natural frequency. It is also common to achieve substantially higher control bandwidths with linear motor drives than with conventional drives which are more limited by the structural dynamics of the ballscrew transmission. This further enhances the stiffness of the linear motor in spite of the reduced system mass.

Feed Drive Control Design for High-Speed Milling

The structural dynamics of a ballscrew feed drive system can have a significant influence on wide bandwidth servomotor performance. The long and slender assembly of the ballscrew, coupling, and rotor creates torsional and axial modes of vibration which can cause servomotor control loop instability and positioning accuracy problems. The axial dynamics are uncoupled from the torsional dynamics for isolated axisymmetric bodies, like the ballscrew, coupling, and rotor assembly. However, the physical constraint imposed by the translational table which is attached to the ballscrew through the ballnut does provide a coupling mechanism between the axial and torsional dynamics of the rotational components. This results from the helical geometry of the ballscrew which couples a force on the ballnut with an axial force and a coaxial moment on the ballscrew. Since the transmission ratio of the ballscrew is usually small, the dynamic coupling between the axial and torsional dynamics is also small and, in many cases, may be neglected for a simplified analysis of the ballscrew feed drive system.

In order to design a robust, wide bandwidth servomotor control system using ballscrew feed drives, it is helpful to develop a dynamic structural model of the drive system. This aids the control system design which must be tolerant of the structural modes in the feed drive mechanism. A model, such as this one, can also be used to identify the

modes which are sensitive to changes in the operating parameters, such as the workpiece mass and the position of the axis.

It has been found that, even a relatively low order structural model with less than 100 degrees of freedom, can provide good results which will reveal the behavior of the ballscrew feed drive system. The dynamics can be modeled using beam type finite elements for the rotational elements, along with a lumped mass for the table and lumped stiffness parameters to tie the model components together. A diagram of the components modeled and the component connectivity is shown in Figure 3-7. A model of this type can be constrained to include the effect of the helical screw which couples the axial and rotational degrees of freedom.

The beam finite elements used for this model have two nodes. Each node has an axial displacement degree of freedom and a rotational displacement degree of freedom. A diagram of the beam element degrees of freedom is shown in Figure 3-8. The beam element stiffness matrix between the four displacement coordinates shown in Figure 3-8 is given by [13]

$$K_{el} = \frac{1}{l}\begin{bmatrix} EA & 0 & -EA & 0 \\ 0 & GJ & 0 & -GJ \\ -EA & 0 & EA & 0 \\ 0 & -GJ & 0 & GJ \end{bmatrix} \begin{matrix} u_1 \\ u_2 \\ u_3 \\ u_4 \end{matrix} \tag{3-12}$$

where:

E = modulus of elasticity of beam material

G = modulus of rigidity of beam material

A = cross-sectional area of beam element

J = polar area moment of inertia of beam element

l = beam element length

The beam element mass matrix between the four displacement coordinates shown in Figure 3-8 is given by [13]

$$M_{el} = \frac{\rho l}{6} \begin{bmatrix} 2A & 0 & A & 0 \\ 0 & 2J & 0 & J \\ A & 0 & 2A & 0 \\ 0 & J & 0 & 2J \end{bmatrix} \begin{matrix} u_1 \\ u_2 \\ u_3 \\ u_4 \end{matrix} \tag{3-13}$$

where:

ρ = density of beam material

The rotor of the brushless DC servomotor has a specified mass moment of inertia, but the manufacturer does not provide any physical dimensions or construction details regarding the rotor. Therefore, estimates of the rotor geometry have been made to develop a dynamic model of the system. An estimate of the rotor length was made based on the physical outside dimensions of the motor. The rotor is known to be constructed of neodymium-iron-boron permanent magnet material bonded around a solid steel shaft. The density of the magnet material is 7400 kg/m^3, which is close to the density of steel (7850 kg/m^3). It is assumed that 60 percent of the total rotor diameter is comprised of the central steel shaft with the surrounding permanent magnet material making up the diameter required to obtain the specified mass moment of inertia.

The ballscrew has a helical groove for the ball elements, which is cut around the periphery of the ballscrew shaft. The ballscrew could be modeled with greater accuracy by using a high order finite element mesh of solid elements. However, due to other

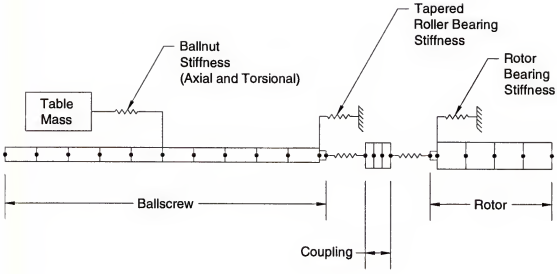

Figure 3-7. Dynamic structural model of a ballscrew feed drive system.

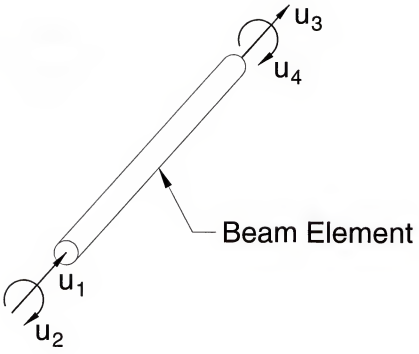

Figure 3-8. Two node beam type finite element with axial and rotational degrees of freedom.

uncertainties in the model such as the lumped stiffness elements for the bearings and the rotor dimensions, it is unjustified to create such a complex model for the ballscrew shaft. The beam finite element model, therefore, assumes that the threads provide minimal stiffness for the ballscrew, although they do significantly contribute to the inertia. The element stiffness matrix for the ballscrew is based on the minor diameter of the ballscrew. The element mass matrix for the ballscrew is based on the average values for the cross-sectional area and the polar area moment of inertia.

The axis table is modeled as a lumped mass which is constrained to translate along the axis guideways and is rigidly attached to the ballnut. The ballnut can be attached to any of the ballscrew finite element nodes with stiffness elements that model the compliance in the ball contact sites between the screw and the nut. The displacement of the table along the guideways adds one additional degree of freedom to the model.

A force diagram for the ballscrew and ballnut contact is shown in Figure 3-9. The ball contact force, F_b, represents the force transmitted by one ball. The recirculating ballnut contains many ball contact points which are distributed around the ballscrew thread. The resultant of all contact forces produces a force component along the axis of the ballscrew and a moment about the axis of the ballscrew. If the screw is well designed, then any resultant radial force or bending moments should be small.

The compliance in the contact between the ball and the ball groove is modeled by a spring element which is oriented normal to the ball groove at the point of contact. This orientation for many contact points provides thrust stiffness and torsional stiffness between the screw and the nut. The stiffness matrix for the ballnut connection between the three degrees of freedom indicated in Figure 3-9 is

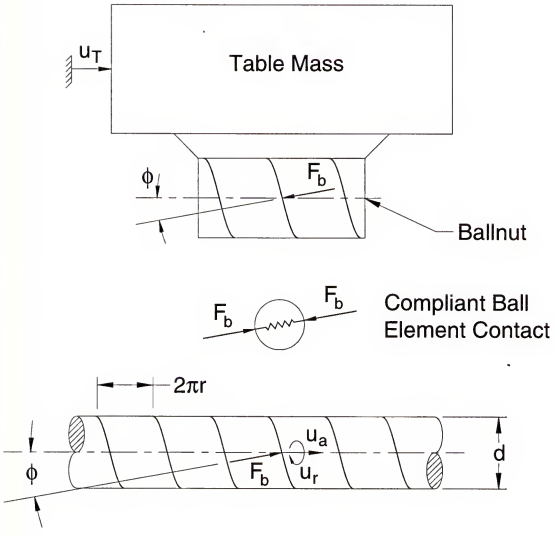

Figure 3-9. Ballscrew and ballnut force diagram.

$$K_{nut} = k_{th} \begin{bmatrix} 1 & -r & -1 \\ -r & r^2 & r \\ -1 & r & 1 \end{bmatrix} \begin{matrix} u_a \\ u_r \\ u_T \end{matrix} \tag{3-14}$$

where:

k_{th} = axial thrust stiffness of the ballnut

r = transmission ratio of ballscrew

Additional lumped spring elements are added to the model to connect the ballscrew, coupling, and rotor together and to model the axial stiffness of the bearings.

A complete dynamic finite element analysis program for the X axis feed drive on the MTRC high-speed milling machine is written in the MATLAB programming language and is included in Appendix A. This model represents the undamped structural dynamics for the feed drive system. The undamped natural modes from the finite element model solution can be combined with measured modal damping ratios to completely describe the structural response of the feed drive system. The model allows only one degree of freedom for the saddle motion. Therefore, only translation of the saddle is permitted and the problem is simplified to one servomotor driving one half of the X axis saddle mass. The model could easily be expanded to include both X axis screws and allow for rotation of the saddle against the guideways.

The modeshapes for the four most important modes in the ballscrew feed drive model are shown in Figure 3-11. The modeshapes for each mode are separated into the axial displacements and rotational displacements. The linear displacement coordinate for the table is marked on each mode with a circled plus sign and is plotted with the axial modeshape. The first mode is a rigid body mode that allows the screw to rotate freely in

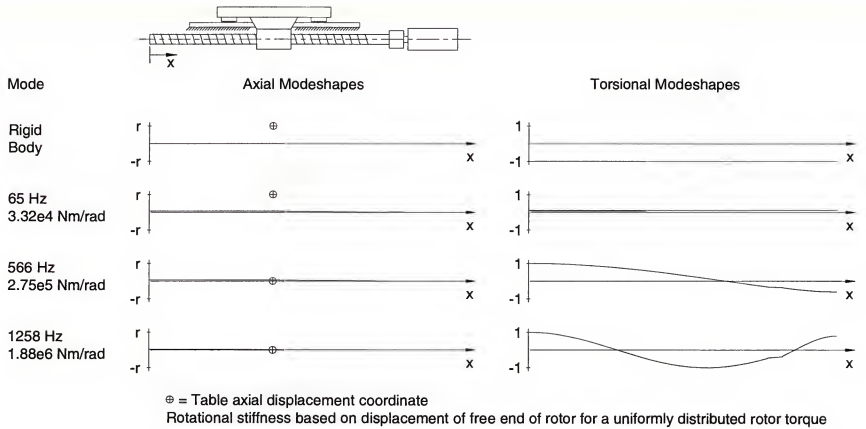

Figure 3-10. Most important modes for the X axis ballscrew feed drive on the MTRC high-speed milling machine. Axial modeshapes are scaled to the ballscrew transmission ratio r.

order to position the axis. The rigid body mode is the only mode that is desirable for a feed drive system since it is the mode that provides useful axis motion. For many conventional bandwidth axes, the rigid body mode is the only mode that must be included in the control system model. When designing wide bandwidth servomotor control, it becomes necessary to consider additional structural modes in the control system model. All four of the modes shown in Figure 3-10 have been found to influence the control system performance on the MTRC machine. Each mode, except for the rigid body mode, is associated with a natural frequency and a torsional stiffness parameter. The torsional stiffness is calculated between rotation at the free end of the rotor and a torque that is uniformly distributed across the rotor. The stiffness parameter is significant for the control system model since the motor field torque is uniformly distributed across the rotor length while the angular velocity of the rotor is fed back from a tachogenerator attached to the free end of the rotor.

The second mode in Figure 3-10, at 65 Hz, can be described as an axial mode where the saddle mass is connected to ground through the axial stiffness of the ballscrew, ballnut, and tapered roller bearings. This mode is lightly coupled between the axial and rotational degrees of freedom. The third and fourth modes of the feed drive system at 566 Hz and 1258 Hz, respectively, show large rotational displacements and are considered to be torsional modes of the feed drive system. In these two modes the axial degrees of freedom are only slightly coupled with the torsional degrees of freedom.

The results obtained from the undamped, finite element model can be combined with modal damping ratios measured on assembled ballscrew feed drives to calculate frequency response behavior of the structure. Measurements indicate that the damping ratio for the mode at 65 Hz, with large displacement of the saddle, should be

approximately 10 percent. The modes that are associated with large torsional displacements have been found to have damping ratios of about 1.0 percent. Using the results from the finite element model and the measured damping ratios, the frequency response between the angular velocity of the free end of the rotor and a uniformly distributed rotor torque can be evaluated as shown in Figure 3-11. This frequency response is significant since it represents the servomotor open-loop response for the velocity control loop. It will be shown in Chapter 5 that the torsional modes of the ballscrew, coupling, and rotor structure can lead to instability of the servomotor control system unless proper compensation is provided within the velocity control loop.

The second mode at 65 Hz, in Figure 3-10, that is predominately the saddle mass moving against the ballscrew, ballnut, and bearing stiffness does not present a stability problem when the position feedback is taken from a rotary encoder attached to the rotor. This mode can be approximated as being external to the position loop in this case since the motion at the rotor is small compared with the displacement of the saddle. However, this mode does lead to dynamic errors in the axis position for wide bandwidth motion commands. Feedforward compensation for these dynamics can be included in the position control loop provided that the feed drive system can be sufficiently modeled. However, this mode may prove to be difficult to model since it is sensitive to the axis mass which depends on the workpiece and because the stiffness of the mode depends on the axis position along the ballscrew.

If the position feedback is taken from a linear scale attached to the saddle, then this axial mode at 65 Hz will be included in the position loop control dynamics. This situation can lead to improved dynamic position performance, as well as creating

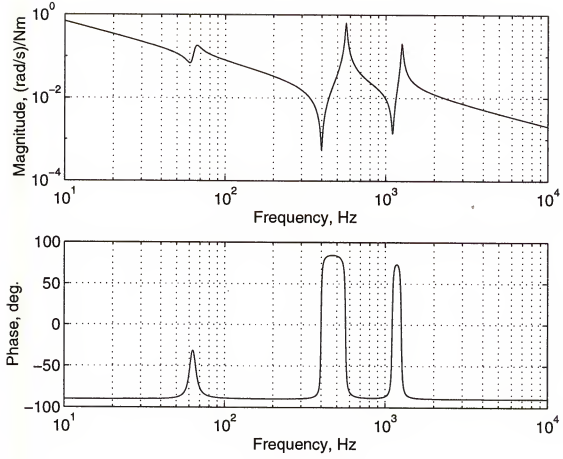

Figure 3-11. Modeled frequency response between the angular velocity at the free end of the rotor and a distributed torque applied uniformly across the rotor.

potentially destabilizing effects for the control system. The dynamics incorporated into the control system from feedback of the saddle position may require additional compensation to maintain stability.

While the leadscrew is, perhaps, the most problematic structural element in a conventional axis feed drive, it is not the only element of concern when operating over wide bandwidths. For example, the saddle (or table) with its associated guideway flexibility may pose similar structural problems. The coupling which joins the rotary encoder to the rotor may also produce a mode that directly affects the position loop stability.

The current trend is to use linear motor technology for high-speed and wide bandwidth servomotor feed drives on linear axes. These motors eliminate the conventional ballscrew transmission and the associated dynamics discussed above. This is an important advantage, since the electromagnetic field directly produces a force on the linear motor rotor which is rigidly attached to the table. However, it is still possible to encounter vibrational modes associated with the table or saddle structure which can create stability problems and dynamic position errors as discussed for the ballscrew feed drive.

CHAPTER 4
WIDE BANDWIDTH AXIS MOTION COMMANDS

The bandwidth requirement for a servomotor position loop depends strongly on the duration of the acceleration portion of the command and on the formulation of the acceleration profile. In high-speed milling of rectangular pocketed structures, the axes must constantly undergo large accelerations and decelerations to rapidly execute the required corner motions. The axes, in this case, are constantly subjected to short duration acceleration pulses in between longer periods of zero acceleration. The acceleration phases of the command represent the largest bandwidth portion of the motion.

The most straightforward acceleration profile is one with a constant acceleration throughout the acceleration portions of the motion. The acceleration in this case is a rectangular pulse. A rectangular pulse signal of duration τ and height A is shown in Figure 4-1a. This signal has a closed form continuous Fourier transform which is

$$Ap_{\tau}(t) \leftrightarrow A\tau e^{-j\frac{\tau\omega}{2}} Sa\left(\frac{\omega\tau}{2}\right) \tag{4-1}$$

where

$$p_{\tau}(t) = \begin{cases} 1 & 0 \le t \le \tau \\ 0 & elsewhere \end{cases}$$

$$Sa(\phi) = \frac{\sin(\phi)}{\phi}$$

A typical high-speed milling motion from rest to 25 m/min with a constant 1.0 g acceleration requires a rectangular acceleration pulse duration of 42.5 ms. The Fourier

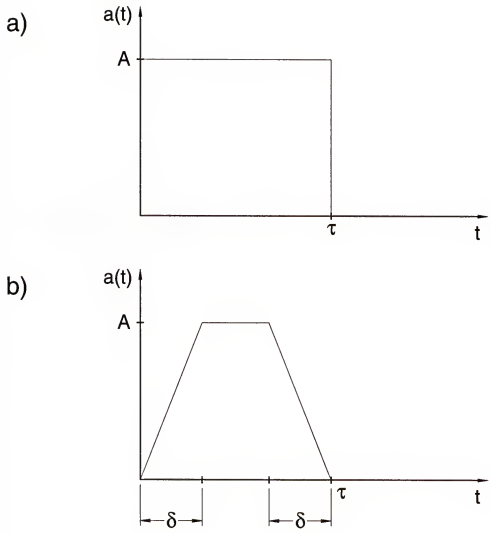

Figure 4-1. Common acceleration signal profiles used for motion commands.
a) Rectangular pulse; b) Trapezoidal pulse.

transform magnitude for a rectangular acceleration signal with this duration and magnitude is plotted in Figure 4-2. The magnitude spectrum contains an infinite series of lobes that are scaled in magnitude with the reciprocal of the frequency. The lobe centered around zero frequency is frequently called the main lobe since it contains most of the signal energy. The other lobes of the spectrum magnitude are called sidelobes. Although most of the energy of the signal is concentrated within the main lobe of the spectrum, the sidelobes roll off rather slowly with increasing frequency for the rectangular pulse signal.

The position control loop performance can be described by its transfer function, which describes the position response of the servomotor, $X(s)$, to the position command, $X_{com}(s)$.

$$\frac{X(s)}{X_{com}(s)} = G_p(s) \tag{4-2}$$

In addition, the same transfer function also describes the servomotor acceleration, $\ddot{X}(s)$, in response to the command acceleration, $\ddot{X}_{com}(s)$.

$$\frac{\ddot{X}(s)}{\ddot{X}_{com}(s)} = G_p(s) \tag{4-3}$$

With this interpretation, it is easy to understand how the servomotor control loop will respond to the commanded axis acceleration. The servomotor acts as a low pass filter for the acceleration command spectrum. Therefore, any frequency content beyond the servomotor control bandwidth will lead to acceleration errors which will correspond to position errors for the servomotor. A position control loop with a 100 Hz bandwidth will accurately track only the frequency components comprised of the mainlobe through the third sidelobe for the acceleration spectrum shown in Figure 4-2.

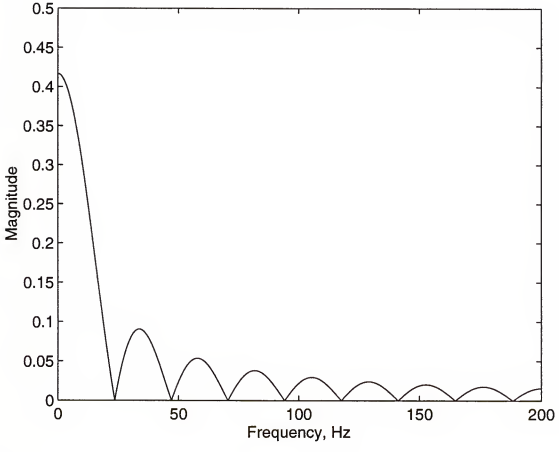

Figure 4-2. Fourier transform magnitude of a rectangular pulse acceleration profile with a 1.0 g magnitude.

Achieving better tracking accuracy is possible by constructing different acceleration profiles that will lead to a steeper roll-off of the spectrum with increasing frequency. This will concentrate more of the command spectrum within the bandwidth of the position control loop. A common method is to use a symmetrical, trapezoidal acceleration profile, as shown in Figure 4-1b, instead of the rectangular profile already considered. This type of acceleration profile can easily be created and is therefore suitable for real-time command generation. The linearly increasing and linearly decreasing acceleration portions of the signal correspond to constant jerk commands. A special case of a trapezoidal profile is a triangular profile ($\delta = \tau/2$), where the acceleration command linearly increases from zero to a peak value and then linearly returns to zero. This signal also has a simple, closed form continuous Fourier transform.

$$A\left\{1-\left|\frac{2t}{\tau}-1\right|\right\}p_\tau(t) \leftrightarrow \frac{A\tau}{2}e^{-j\frac{\tau\omega}{2}}Sa^2\left(\frac{\omega\tau}{4}\right) \tag{4-4}$$

The magnitude of the Fourier transform for a triangular acceleration profile, with a 42.5 ms duration and a 1.0 g average acceleration, is shown in Figure 4-3. The triangular acceleration profile, with a 1.0 g average acceleration, will have a 2.0 g peak acceleration. It is apparent from Figures 4-2 and 4-3 and from Equations 4-1 and 4-4 that the lobes are twice as wide for the triangular acceleration signal. More importantly, however, the spectrum magnitude rolls off much more rapidly with increasing frequency for the triangular profile. This means that the position control loop will more accurately track this command signal than when the acceleration is generated as a rectangular pulse. The drawback to using this form of acceleration command is that it requires twice the peak acceleration to maintain the same average acceleration as can be obtained by using a

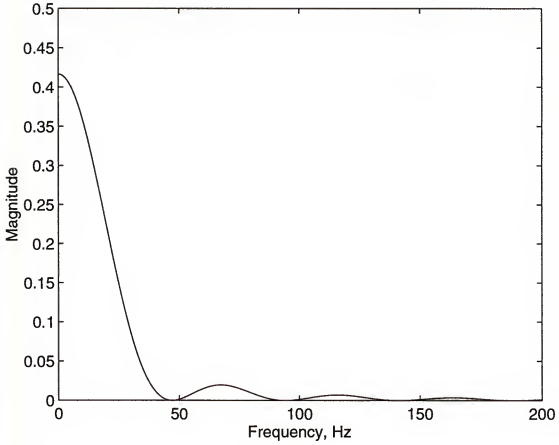

Figure 4-3. Fourier transform magnitude of a triangular pulse acceleration profile with a 2.0 g peak acceleration.

rectangular profile. The general trapezoidal acceleration profile which has a constant acceleration portion will require a peak acceleration that lies between the average acceleration and two times the average acceleration. The side lobe roll-off will also lie in between the two extremes given for the rectangular and triangular acceleration profiles.

It is insightful to evaluate the acceleration response, in the time domain, to the rectangular and the triangular acceleration profiles. To perform this analysis, the position loop transfer function will be assumed to have the following second order form

$$G_p(s) = \frac{\omega_n^2}{s^2 + 2\zeta\omega_n s + \omega_n^2} \tag{4-5}$$

where:

ω_n = position loop natural frequency

ζ = position loop damping ratio

For evaluation purposes the natural frequency will be assumed to be 100 Hz and the damping ratio will be chosen to be 0.7. The acceleration response to an acceleration command with a step profile of 1.0 g with a pulse duration of 42.5 ms is shown in Figure 4-4a. This clearly shows the step response of a second order system with relatively large errors near the step transitions. The response to the triangular acceleration profile with a 1.0 g average acceleration is shown in Figure 4-4b. The shape of the acceleration response much more closely resembles the shape of the triangular acceleration command than does the response to the step acceleration profile. There is a noticeable time delay between the command and the response but this does not present a problem for accuracy of the motion, as will be explained in Chapter 7. On the other hand, the distortion of the commanded acceleration profile for the step acceleration command does represent motion

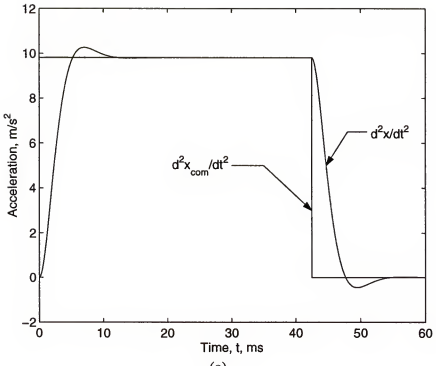

(a)

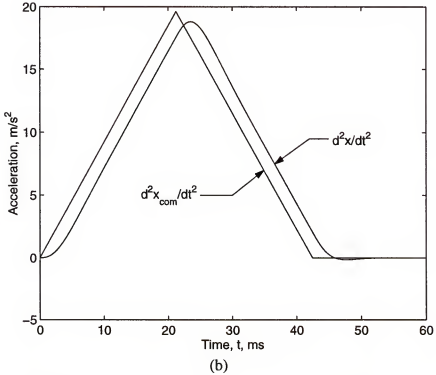

(b)

Figure 4-4. Acceleration response to commands with 1.0 g average acceleration.
a) Step acceleration profile; b) Triangular acceleration profile.

errors. It will also be shown in Chapter 7 that the time delay, T_d, associated with the transfer function given by Equation 4-5 is

$$T_d = \frac{2\zeta}{\omega_n} \tag{4-6}$$

The acceleration responses shown in Figure 4-4 are plotted with delayed versions of the acceleration commands in Figure 4-5. In this figure, it is apparent that the triangular acceleration command profile will provide a substantial improvement in the motion accuracy.

It is possible to design other acceleration profiles that have even smaller sidelobes than the triangular profile, but these tend to have rather complicated formulations which are not as suitable for real-time command generation. It is most common, therefore, to implement the trapezoidal acceleration formulation to reduce the sidelode magnitudes and to improve the position tracking performance.

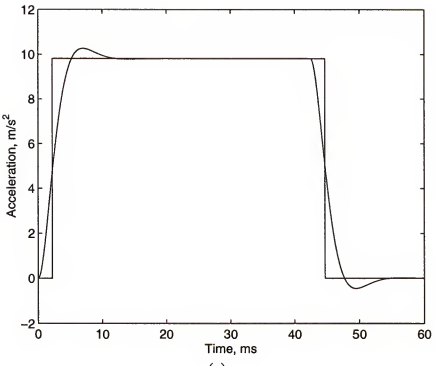

(a)

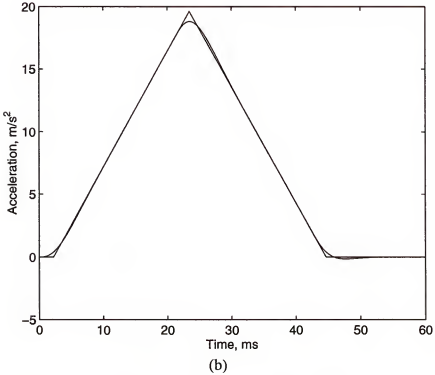

(b)

Figure 4-5. Acceleration response plotted with delayed commands.
a) Step acceleration profile; b) Triangular acceleration profile.

CHAPTER 5
WIDE BANDWIDTH CONTROL OF CONVENTIONAL BALLSCREW FEEDRIVES

Achieving position loop control bandwidths of 100 Hz or greater usually requires careful compensation of structural vibration modes that exist in the feed drive components. Compensation of these control loops often involves internal stabilization of the feedback loops and feedforward compensation for structural components that are outside of the feedback loop. These structural modes tend to have low damping ratios (0.5 - 3 percent) with a correspondingly large resonant response. Frequently, these modes are also time-varying due to the decreasing mass of the part as it is being machined or as a result of stiffness changes and mass distribution changes with the position of the machine axes.

Measured Structural Dynamics on a Ballscrew Feed Drive

An example of the type of structural modes that are typically encountered with wide bandwidth ballscrew feed drives can be found on the X and Y axes of the MTRC machine. The measured torsional modeshapes for the first two torsional modes of the feed drive system composed of the ballscrew, coupling, and rotor for the X axis are shown in Figure 5-1. These two modes compare with the third and fourth modes, respectively, from Figure 3-10 in Chapter 3 which was created from a finite element model of the X axis ballscrew feed drive. These modes are associated with small structural, damping ratios that result in highly resonant peaks in the servomotor frequency response. The measured,

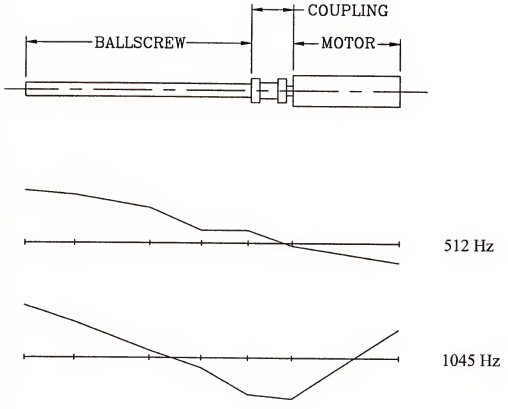

Figure 5-1. Measured torsional modes associated with the rotor, coupling, and ballscrew system.

open-loop frequency response between the tachogenerator signal and the current command signal to the servomotor power amplifier is shown in Figure 5-2. This frequency response measurement is similar to the one based on the finite element model of the X axis feed drive, which was shown in Figure 3-11 of Chapter 3. The measured frequency response includes the effects of analog lowpass filters applied to the amplifier input and to the tachogenerator output as well as the structural response of the feed drive system. The lowpass filters cause an additional phase lag that was not included in the structural frequency response based on the finite element model of the feed drive structure. Without proper compensation, these torsional modes will cause instability, or limit the position loop bandwidth to an unacceptably low value. Fortunately, these torsional modes are relatively insensitive to the table (saddle) mass; thus in this case, it is possible to design effective compensation without concern for the workpiece mass or the table position.

Design of Wide Bandwidth Axis Control for Ballscrew Feed Drives

A block diagram of the position control system for both the X axis and the Y axis of the MTRC machine is shown in Figure 5-3. The feedback of position comes from a rotary encoder, that is coupled to the servomotor rotor. An analog tachogenerator is used to establish position loop damping via the internal velocity loop. Since the velocity loop uses samples of the tachogenerator feedback signal, it is necessary to prefilter the feedback signal with a lowpass filter before sampling to prevent signal aliasing. The servomotor power amplifier also uses a lowpass filter on the input to prevent aliasing and to reject high frequency noise before generating the PWM output voltage to the motor. While these lowpass filters are beneficial for preventing signal aliases, they do cause a

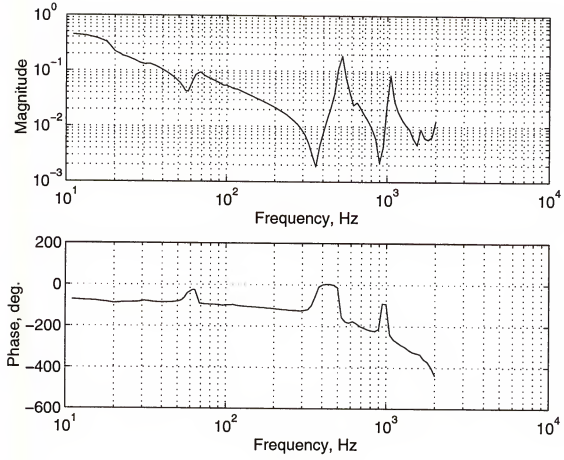

Figure 5-2. Open-loop servomotor frequency response measured between the servo amplifier input tachogenerator output.

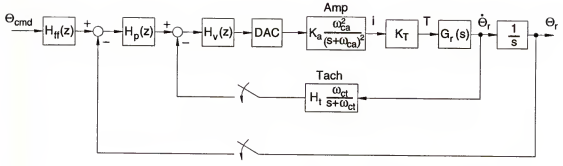

$H_{ff}(z)$ Feedforward compensation
$H_p(z)$ Position loop compensation
$H_v(z)$ Velocity loop compensation
$G_r(s)$ Servomotor transfer function - angular velocity / motor torque

Figure 5-3. Position loop block diagram for the X and Y axes of the MTRC machine.

phase lag that is undesirable for feedback control systems. Therefore, the use of lowpass filters must be weighed against the destabilizing effect that they have on the control system. Since these filters are necessary for establishing the stability of the feedback control system they are included in the block diagram model.

Since the velocity and position loops are sampled data control systems, it is appropriate to develop discrete-time transfer functions for the continuous-time models of the servomotor, for the feed drive structure, and for the analog filters. It is possible to define discrete-time transfer functions that exactly represent the samples of the output of the continuous-time system when it is driven by a zero-order hold type digital-to-analog converter, as shown by Franklin, Powell and Workman [14]. The discrete equivalent transfer function for the elements from the current mode, servomotor amplifier control voltage to the tachogenerator output signal is given by

$$G_v(z) = \left(\frac{z-1}{z}\right) Z\left\{ L^{-1}\left[\frac{K_a K_T H_t}{s}\left(\frac{\omega_{ca}^2}{s+\omega_{ca}^2}\right)\left(\frac{\omega_{ct}}{s+\omega_{ct}}\right) G_r(s)\right]\Bigg|_{t=kT}\right\} \tag{5-1}$$

where:

$G_v(z)$ = discrete-time equivalent transfer function from servomotor amplifier control input to tachogenerator output signal

$G_r(s)$ = servomotor transfer function between the rotor angular velocity and the rotor torque (includes structural dynamics of feed drive system)

Z = Z transform operator

L^{-1} = Inverse Laplace transform operator

k = discrete-time sample index

T = sampling period

Similarly, the discrete equivalent transfer function from the amplifier input to the position encoder output is given by

$$G_p(z) = \left(\frac{z-1}{z}\right) Z\left\{ L^{-1}\left[\frac{K_a K_T}{s^2}\left(\frac{\omega_{ca}^2}{s+\omega_{ca}^2}\right) G_r(s) \right] \Bigg|_{t=kT} \right\} \tag{5-2}$$

where:

$G_p(z)$ = discrete-time equivalent transfer function from amplifier input to encoder

The position loop block diagram can be rewritten in terms of the discrete equivalent transfer functions given by Equations 5-1 and 5-2 to provide an entirely discrete-time control system model. The block diagram for this model is shown in Figure 5-4. The discrete-time position loop model is used as the basis for the control system design.

In order to analyze the stability of the servomotor control system and to design a stabilizing compensator, it is essential to develop a model of the transfer function, $G_r(s)$, which relates the motor torque to the angular velocity of the rotor. It is obvious that the transfer function must have a rigid body rotation mode, since there is no torsional connection to ground. This mode is always included in servomotor control models since it represents the useful motion of the servomotor. The rigid body mode resists rotation through the total mass moment of inertia of the feed drive system. For conventional bandwidth control systems, the rigid body mode is the only important mode in the feed drive system. In this case, the control system design is greatly simplified. However, for the wide bandwidth servomotor control necessary for high-speed milling, the transfer function model, $G_r(s)$, must include the effects of additional vibration modes. Based on the finite

element modeling results from Chapter 3 and the measured frequency response shown in Figure 5-2, it is appropriate to include two additional normal modes in the transfer function model. The prototype transfer function is given by

$$G_r(s) = \frac{1}{Js} + \frac{1}{k_1}\frac{\omega_{n1}{}^2 s}{s^2 + 2\zeta_1\omega_{n1}s + \omega_{n1}{}^2} + \frac{1}{k_2}\frac{\omega_{n2}{}^2 s}{s^2 + 2\zeta_2\omega_{n2}s + \omega_{n2}{}^2} \tag{5-3}$$

where:

J = mass moment of inertia of drive system including equivalent inertia of table

k_i = torsional stiffness of rotational mode i

ζ_i = damping ratio of rotational mode i

ω_{ni} = natural frequency of rotational mode i

It is impractical to use Equation 5-3 to symbolically evaluate the discrete equivalent transfer function given by Equation 5-1. It is, therefore, necessary to substitute numerical values before going any further with the modeling of the position loop control system. The transfer function modal parameters for the feed drive structure that are needed to evaluate Equation 5-3 are determined from the frequency response measurement shown in Figure 5-2. The remaining parameters needed to evaluate the discrete equivalent transfer function given by Equation 5-1 are obtained from data supplied by the manufacturers of the individual components. The values for all parameters required to evaluate the discrete-time equivalent transfer function of Equation 5-1 are given in Table 5-1. The numerical evaluation of the discrete-time transfer function, $G_v(z)$, is

$$G_v(z) = 0.00178\frac{(z^2 - 1.7333z + 0.98616)(z^2 - 0.64769z + 0.95707)}{(z-1)(z^2 - 0.23261z + 0.94361)(z^2 - 1.4943z + 0.97196)} \times \frac{(z + 0.34405)(z + 3.5644)(z + 0.029251)}{(z^2 - 0.49886z + 0.062214)(z - 0.062214)} \tag{5-4}$$

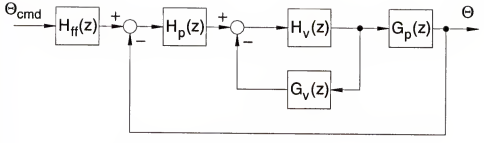

$H_{ff}(z)$ Feedforward compensation
$H_p(z)$ Position loop compensation
$H_v(z)$ Velocity loop compensation
$G_v(z)$ Discrete transfer function - Tach output / Amp input
$G_p(z)$ Discrete transfer function - Encoder output / Amp input

Figure 5-4. Discrete-time position loop block diagram for the X and Y axes of the MTRC machine.

Table 5-1. Parameters used to evaluate the discrete-time transfer function $G_v(z)$

Parameter	Value	Description
K_a	15.1 A/V	transconductance servo amplifier gain
K_T	1.646 Nm/Arms	D.C. motor torque constant
H_t	0.0477 V/(rad/s)	tachogenerator sensitivity
ω_{ca}	6300 rad/s	servo amplifier input lowpass cutoff filter frequency
ω_{ct}	12600 rad/s	antialias lowpass filter cutoff frequency
J	0.0304 kg m^2	total mass moment of inertia for the feed drive
k_1	3.80e5 Nm/rad	stiffness of torsional mode 1
ω_{n1}	3220 rad/s	natural frequency of torsional mode 1
ζ_1	0.02	damping ratio of torsional mode 1
k_2	1.52e6 Nm/rad	stiffness of torsional mode 2
ω_{n2}	6570 rad/s	natural frequency of torsional mode 2
ζ_2	0.02	damping ratio of torsional mode 2
T	221 μs	discrete-time control sampling period

The discrete-time transfer function $G_p(z)$ evaluated using Equation 5-2 is

$$G_p(z) = 4.95 \times 10^{-6} \frac{(z^2 - 1.7332z + 0.98599)(z^2 - 0.64782z + 0.95548)}{(z^2 - 0.23261z + 0.94361)(z^2 - 1.4943z + 0.97196)} \times \frac{(z - 0.24943)^2 (z + 5.7009)(z + 0.58596)(z + 0.056226)}{(z - 1)^2 (z^2 - 0.49886z + 0.062214)^2} \quad (5\text{-}5)$$

The frequency response of the discrete-time transfer function model is obtained by substituting $z = e^{j\omega T}$ into Equation 5-4, where ω is the radian frequency variable and T is the control system sampling period. The frequency response of the model, $G_v(e^{j\omega T})$, is shown in Figure 5-5 and is plotted along with the measured response previously presented

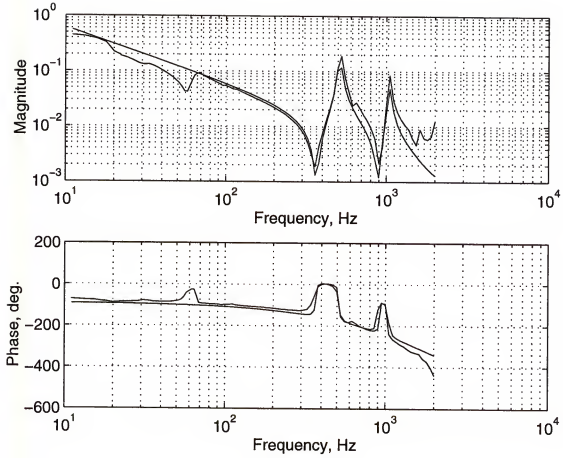

Figure 5-5. Comparison of modeled and measured frequency response between the servo amplifier input and the tachogenerator output.

in Figure 5-2. This comparison shows that the model should be sufficiently accurate for control system design; however, the model could probably be slightly improved by optimizing the complex poles and zeros of $G_v(z)$ to obtain a better agreement with the measured response.

Based on the Nyquist stability criterion, the frequency response indicates that the two torsional modes may create instability in the velocity loop if the loop is closed using only a large proportional gain for $H_v(z)$. The gain margin for the uncompensated velocity loop is only 16.7. Any proportional controller with a gain greater than this will result in instability. If the velocity loop gain is limited to this value, then the closed-loop bandwidth would be less than 10 Hz for the velocity loop. This would be unacceptable for high-speed milling applications; therefore, some method of control system compensation must be applied to improve the performance of the feed drive.

One reasonable approach to stabilizing this control system is to use a lag or a lowpass filter compensation to attenuate the resonances of the torsional modes. This is the typical method used to contend with these types of modes, and it does allow a greater closed-loop bandwidth than using only the proportional gain alone. However, this still limits the velocity loop bandwidth more than is acceptable for high-speed milling applications. An alternative approach is to apply a modal compensation filter to the undesirable modes and, thus, cancel the effects of the torsional dynamics. This provides closed-loop stability for the velocity loop at a higher gain and wider bandwidth than is possible with the lowpass filter compensation method.

A pole and zero plot for the open-loop transfer function, $G_v(z)$, in the Z plane is shown in Figure 5-6. There are four complex poles and four complex zeros near the unit

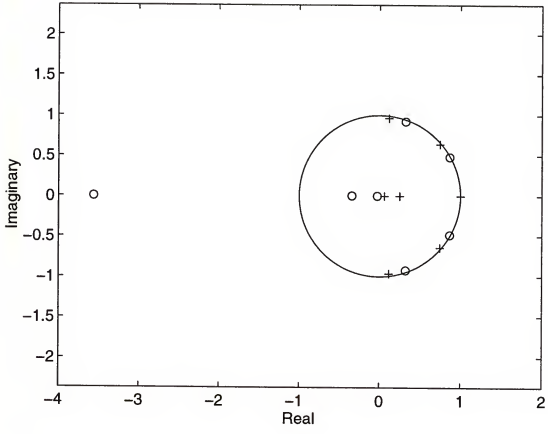

Figure 5-6. Pole and zero map for the transfer function $G_v(z)$.

circle that are associated with the lowly damped torsional modes. The velocity loop compensation strategy is to design $H_v(z)$ in order to essentially cancel these poles and zeros. The zeros $H_v(z)$ are chosen to exactly match the four lowly damped poles of $G_v(z)$. This attenuates the resonances in $G_v(z)$, however, these four zeros will lead to excessive high frequency gain and phase lift unless additional poles are included in the compensation transfer function, $H_v(z)$. The poles of $H_v(z)$ are specified to be at the same angle as the four undesirable zeros of $G_v(z)$, but the magnitude of the poles are chosen to be about 2 percent smaller than the magnitude of the zeros of $G_v(z)$. This choice for the pole locations decreases and broadens the resonant response of the compensation near the poles. This cancellation compromise adds a level of robustness against parameter uncertainty and against changes in the frequency response. The undesirable poles and zeros of $G_v(z)$ and the compensating poles and zeros of $H_v(z)$ are listed in Table 5-2 in polar form. The compensation transfer function $H_v(z)$ designed according to this method is

$$H_v(z) = 7.03\frac{(z^2 - 0.23261z + 0.94361)(z^2 - 1.49430z + 0.97196)}{(z^2 - 0.63474z + 0.91917)(z^2 - 1.69863z + 0.94711)} \tag{5-6}$$

The frequency response of the compensation filter, $H_v(e^{j\omega T})$, is shown in Figure 5-7.

The effectiveness of applying this pole and zero canceling compensation can be seen in Figure 5-8, which shows the measured open-loop frequency response for the velocity loop with the compensation filter, $H_v(z)$, implemented. With this compensation applied in the velocity loop, the control system behaves as if the torsional modes did not exist. The position loop can then be closed using only a proportional gain of $H_p(z) = 17$ to achieve a bandwidth of 100 Hz.

Table 5-2. Locations of the velocity loop compensation poles and zeros.

Undesirable Poles and Zeros of $G_v(z)$				Compensation Poles and Zeros of $H_v(z)$			
Poles		Zeros		Poles		Zeros	
Radius	Angle (rad)	Radius	Angle (rad)	Radius	Angle (rad)	Radius	Angle (rad)
0.98588	+0.7108	0.99306	+0.5101	0.97319	+0.5101	0.98588	+0.7108
0.98588	−0.7108	0.99306	−0.5101	0.97319	−0.5101	0.98588	−0.7108
0.97139	+1.4508	0.97830	+1.2334	0.95873	+1.2334	0.97139	+1.4508
0.97139	−1.4508	0.97830	−1.2334	0.95873	−1.2334	0.97139	−1.4508

The closed position loop transfer function based on the control system block diagram shown in Figure 5-4 and the transfer functions developed in this chapter is

$$G_{pl}(z) = \frac{(z+5.7009)(z+0.58596)(z+0.056226)(z-0.062214)}{(z-0.64989)(z^2-1.78178z+0.89613)(z^2-0.13015z+0.092236)} \times \frac{(z^2-0.64782z+0.97749)(z^2-1.73320z+0.99297)}{(z^2-0.63213z+0.95810)(z^2-1.68740z+0.96555)} \tag{5-7}$$

The position loop frequency response for the control system model, $G_{pl}(e^{j\omega T})$, is shown in Figure 5-9. The measured frequency response of the position loop control system on the MTRC high-speed milling machine is shown in Figure 5-10 for comparison with the control system model.

While the servomotor control bandwidth reaches 100 Hz, the ballscrew feed drive has structural modes with natural frequencies less than 100 Hz that are outside of the position loop when position feedback is taken from a position encoder on the rotor. These are modes that have modeshapes with, predominately, axial displacements such as the second mode in Figure 3-10. These modes do not cause stability problems, but they do lead to dynamic errors in position when attempting to execute wide bandwidth motions.

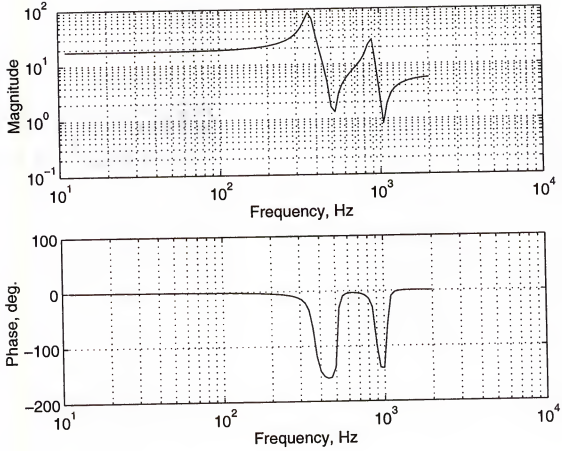

Figure 5-7. Frequency response of velocity loop compensation filter $H_v(z)$.

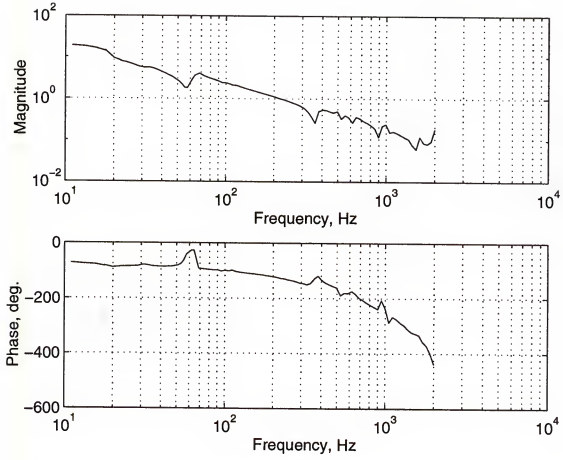

Figure 5-8. Frequency response of velocity loop compensator, $H_v(z)$, applied to the measured open-loop frequency response from the servomotor amplifier input to the tachogenerator output.

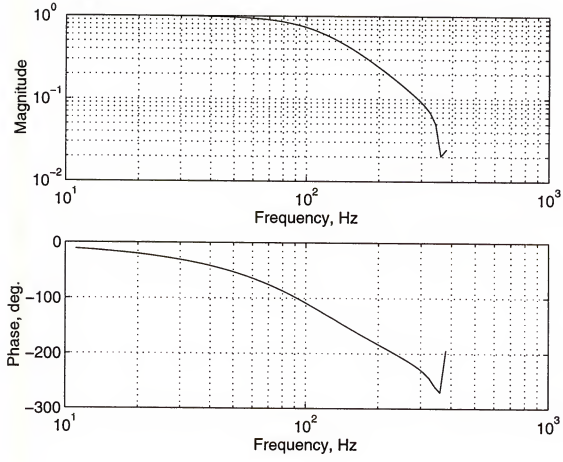

Figure 5-9. Modeled frequency response of closed position loop at the rotary encoder.

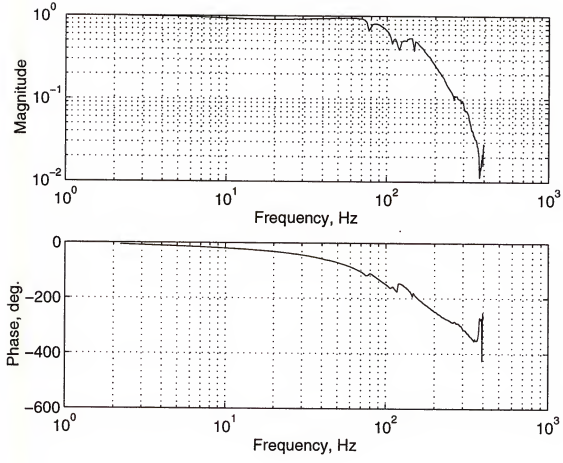

Figure 5-10. Measured frequency response of closed position loop at the rotary encoder.

The effect of these modes can be seen by measuring the frequency response between the axis command signal and the actual axis position.

The frequency response between the servomotor command signal and a capacitance gage that was used to measure the table position is shown in Figure 5-11. This measurement shows a resonance near 75 Hz that is not seen in the position loop frequency response measurement of Figure 5-10 which is measured from the rotor position.

It may be possible to consider compensating these modes by implementing feedforward compensation based on dynamic models of the feed drive system. However, these models will have to accommodate for the changing dynamics that result from variations in the workpiece mass and the constantly changing position of the ballnut relative to the ballscrew which affects the drive stiffness. Additionally, a compounded axis, such as the X and Y axes of the MTRC machine, will experience a change in the mass distribution as the axis which is carried by the other axis moves over its range of travel. These effects which alter the feed drive dynamics make feedforward compensation a very challenging task for this feed drive system.

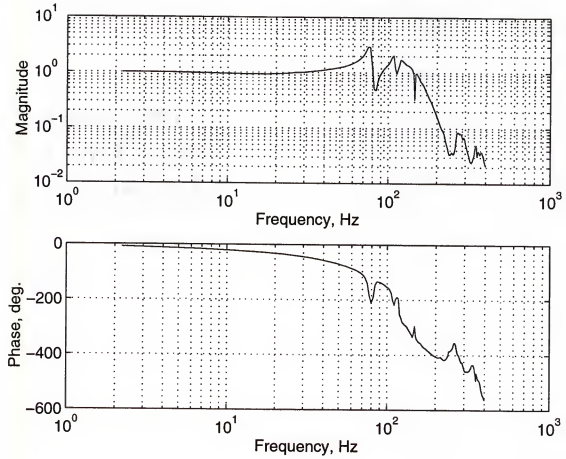

Figure 5-11. Measured frequency response of closed position loop at the table.

CHAPTER 6
CONTROL OF YAW ERROR ON FEEDRIVES WITH MULTIPLE, NONCOLINEAR MOTORS

In the design of linear machine tool axes, it is highly desirable for the force produced by the servomotor to have a line of action that is parallel to the guideways and that passes through the mass center of the axis. An axis designed in this manner will accelerate in the desired direction without placing any additional loads on the guideways. Axes that use multiple motors should produce a resultant force with the same line of action. Unfortunately, in many applications, the line of action of the motor force does not pass through the axis mass center. This may be the result of a design compromise or due to a mass distribution change during operation of the machine. The changing mass center commonly occurs on a compounded pair of axes where movement of the carried axis changes the center of mass for the other axis. For example, movement of the Y axis table on the MTRC machine changes the mass center of the X axis saddle. During axis accelerations, the compounded axis configuration leads to unwanted rotations that must be resisted by the guideways of the machine. The problem is most severe in high-acceleration axes with a resultant motor force that is applied far from the mass center of the axis.

The X axis of the MTRC machine is driven by two rotary servomotors through ballscrew transmissions. The position feedback is obtained from rotary encoders on the rotors of the servomotors, and the two position loops are closed independently for each motor as if each motor were isolated from the other motor. In reality, there is a structural

coupling in the axis that causes a force developed by one motor to cause a displacement at the driving point for the other motor. Since the Y axis table is carried by the X axis saddle in this configuration, the X axis of the machine will experience a significant redistribution of inertia as the table moves over the full range of motion. On the MTRC machine, the saddle and table masses represent a rather small portion of the total drive inertia due to the small ballscrew transmission ratio. The inertia of the various feed drive components can be seen in Table 6-1. Therefore, the change in position loop performance between the two motors is slight as the Y axis table moves over the full range of motion.

Table 6-1. Mass moment of inertia of components in X axis feed drive.

Component	Mass Moment of Inertia (kg m^2)	Percentage of Total
Rotor	0.0084	27.3
Coupling	0.0048	15.6
Ballscrew	0.0142	46.1
(Saddle + Table)/2	0.0034	11.0
Total	0.0308	100

Although the servomotor performance is rather insensitive to the Y axis position, there will still be dynamic errors of position and yaw on the X axis due the structural modes that are external to the position loop. The yaw errors associated with the conventional ballscrew feed drive will not be pursued any further at this point. Instead, the yaw sensitivity of the X axis saddle to the cross axis table position for the increasingly popular linear servomotor drives will be investigated.

Linear motor drives have become a popular choice for wide bandwidth, high-speed, and high-acceleration feed drives. Wide bandwidth position loop response is

usually more easily achieved by elimination of the structural dynamics associated with the conventional ballscrew transmission. The linear motor can also operate at higher speeds and higher accelerations than a ballscrew and ballnut can tolerate. The substantially higher cost of linear motors, when compared with conventional feed drives, seems to be the greatest drawback to using linear motor technology. When conventional ballscrew feed drives can provide the necessary performance, they will usually be less expensive than equivalent linear motor designs.

It is well known that the servomotor control for a linear motor is usually much more sensitive to changes in the table and workpiece masses than for a rotary servomotor. This is a result of the table and workpiece being the dominant inertia for a linear motor drive whereas it is usually only a small portion of the inertia for the rotary motor and ballscrew drive system. This is evident in Table 6-1, where the saddle and table represent only 11 percent of the total drive inertia for the X axis of the MTRC machine which is a ballscrew axis design.

A two degree-of-freedom model of a dual, linear motor feed drive has been developed to investigate the yaw errors encountered during wide bandwidth and high-acceleration operation. The model is based on the compounded X and Y axes of the MTRC machine with the rotary motors and ballscrew drives replaced by linear motors suitable for 2 g peak acceleration on these axes. The model of the X axis saddle and Y axis table is shown in Figure 6-1. The model includes the guideway stiffness against yaw rotation for the X axis and allows the table to be placed at any location within the allowable Y axis motion. The forces, f_1 and f_2, in Figure 6-1, represent the forces developed by the linear motors. The displacements, x_1 and x_2, represent the positions of

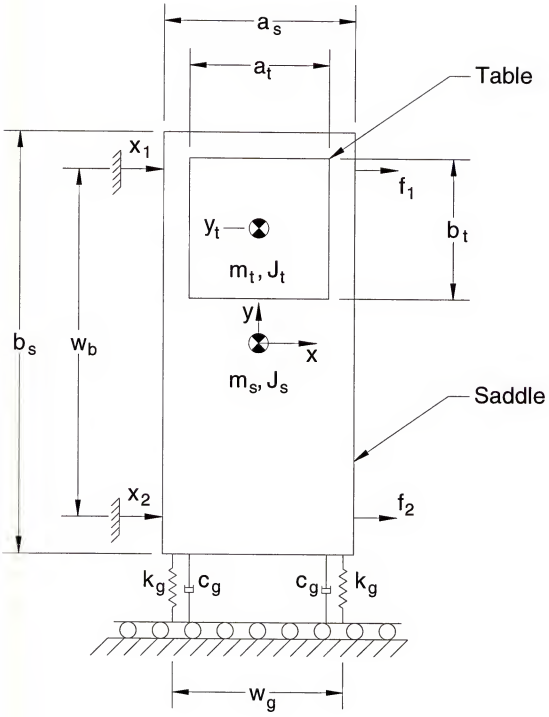

Figure 6-1. Structural model of compounded axes.

the linear motor rotors. The values of the model parameters identified in Figure 6-1 are given in Table 6-2.

Table 6-2. Model parameters for compounded X and Y axes.

Parameter	Value	Description
m_s	450 kg	mass of saddle
m_t	350 kg	mass of table and workpiece
y_t	$-0.4\text{m} \le y_t \le +0.4$ m	location of table relative to saddle center of mass
a_s	530 mm	width of saddle
b_s	1525 mm	height of saddle
a_t	710 mm	width of table
b_t	710 mm	height of table
w_b	790 mm	separation distance between linear servomotors
w_g	375 mm	separation distance between roller carriages
k_g	200 N/μm	roller carriage contact stiffness
c_g	28300 N/(m/s)	roller carriage contact damping constant

The matrix differential equation of motion for the two degree-of-freedom saddle and table structure shown in Figure 6-1 can be expressed by

$$M\ddot{x}(t) + C\dot{x}(t) + Kx(t) = f(t) \tag{6-1}$$

where:

$$M = \begin{bmatrix} (m_s + m_t)\left(\frac{1}{2} + \frac{y_c}{w_b}\right)^2 + \frac{J_c}{w_b^2} & (m_s + m_t)\left[\frac{1}{4} - \left(\frac{y_c}{w_b}\right)^2\right] - \frac{J_c}{w_b^2} \\ (m_s + m_t)\left[\frac{1}{4} - \left(\frac{y_c}{w_b}\right)^2\right] - \frac{J_c}{w_b^2} & (m_s + m_t)\left(\frac{1}{2} - \frac{y_c}{w_b}\right)^2 + \frac{J_c}{w_b^2} \end{bmatrix} = \text{Mass Matrix}$$

$$C = \begin{bmatrix} \frac{c_g}{2}\left(\frac{w_g}{w_b}\right)^2 & -\frac{c_g}{2}\left(\frac{w_g}{w_b}\right)^2 \\ -\frac{c_g}{2}\left(\frac{w_g}{w_b}\right)^2 & \frac{c_g}{2}\left(\frac{w_g}{w_b}\right)^2 \end{bmatrix} = \text{Damping Matrix}$$

$$K = \begin{bmatrix} \frac{k_g}{2}\left(\frac{w_g}{w_b}\right)^2 & -\frac{k_g}{2}\left(\frac{w_g}{w_b}\right)^2 \\ -\frac{k_g}{2}\left(\frac{w_g}{w_b}\right)^2 & \frac{k_g}{2}\left(\frac{w_g}{w_b}\right)^2 \end{bmatrix} = \text{Stiffness Matrix}$$

$$f(t) = \begin{bmatrix} f_1(t) \\ f_2(t) \end{bmatrix} = \text{Linear Motor Force Vector}$$

$$x(t) = \begin{bmatrix} x_1(t) \\ x_2(t) \end{bmatrix} = \text{Rotor Displacement Vector}$$

The combined saddle and table mass center location, y_c, and the mass moment of inertia, J_c, about y_c in Equation 6-1 are related to the table mass center position y_t by

$$y_c = \frac{m_t}{m_s + m_t} y_t \tag{6-2}$$

and

$$J_c = [J_s + m_s y_c^2] + [J_t + m_t (y_t - y_c)^2] \tag{6-3}$$

where J_s and J_t are the mass moments of inertia about the mass centers of the saddle and table, respectively. The component mass moments of inertia used for modeling purposes assume that the mass is uniformly distributed over the rectangular dimensions of the saddle and table components.

$$J_s = \frac{m_s}{12}(a_s^2 + b_s^2) \tag{6-4}$$

$$J_t = \frac{m_t}{12}(a_t^2 + b_t^2) \tag{6-5}$$

The Laplace transform of Equation 6-1, with zero initial conditions, is given by

$$[Ms^2 + Cs + K]X(s) = F(s) \tag{6-6}$$

where $X(s)$ and $F(s)$ are the Laplace transforms of the displacement vector, $x(t)$, and the force vector, $f(t)$, respectively.

Solving Equation 6-6 for $X(s)$ leads to a transfer matrix description of the saddle and table structure which is given by

$$X(s) = [Ms^2 + Cs + K]^{-1}F(s) = \begin{bmatrix} G_{1,1}(s) & G_{1,2}(s) \\ G_{2,1}(s) & G_{2,2}(s) \end{bmatrix} F(s) \tag{6-7}$$

The transfer matrix elements for the structural model can be expressed as

$$G_{i,j}(s) = \frac{\left[\frac{1}{2}(m_s + m_t)\left(2\frac{y_c}{w_b} + (-1)^i\right)\left(2\frac{y_c}{w_b} + (-1)^j\right) + 2\frac{J_c}{w_b^2}\right]s^2 + \left(\frac{w_g}{w_b}\right)^2 c_g s + \left(\frac{w_g}{w_b}\right)^2 k_g}{(m_s + m_t)\left[2\frac{J_c}{w_b^2}s^2 + \left(\frac{w_g}{w_b}\right)^2 c_g s + \left(\frac{w_g}{w_b}\right)^2 k_g\right]s^2} \tag{6-8}$$

This equation defines the motion of the axis saddle in response to the forces applied by the two linear motors.

One common method of controlling the servomotors on this type of axis is to feed back the rotor positions and close separate position loops for each motor as shown in the block diagram of Figure 6-2. This control scheme will be referred to as the independent position loop control (IPLC) system. The parameters K_p, K_v, and H represent control system gains that determine the closed-loop performance of the axis. The gain K_a

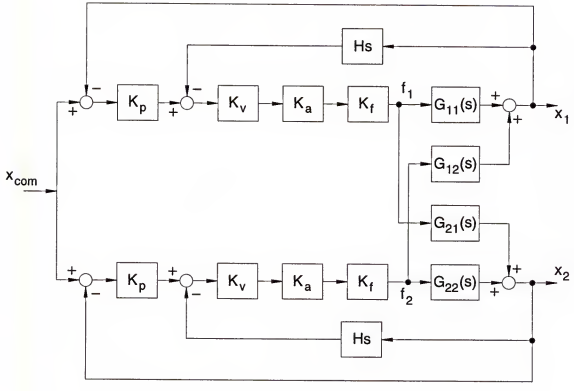

Figure 6-2. Block diagram of a continuous-time, dual, linear servomotor feed drive system.

represents a wide bandwidth transconductance servo amplifier. The gain K_f is the linear motor force constant. However, the two position control loops are not independent, due to the structural coupling that links a force on one rotor with a displacement of the other rotor. This coupling effect is evident by the cross transfer function terms, $G_{1,2}(s)$ and $G_{2,1}(s)$, given in Equation 6-7. The block diagram in Figure 6-2 depicts the coupling that exists between the two position feedback loops.

The block diagram in Figure 6-2 indicates that the velocity loop feedback comes from exact differentiation of the rotor positions. Perfect differentiation is not achievable in any system, although it may be a realistic modeling assumption over a limited bandwidth. For servomotor control, it is usually found to be unnecessary, and undesirable, to differentiate the position feedback signal for frequencies above approximately ten times the velocity loop bandwidth. Beyond this frequency limit, the velocity loop feedback gain should level off or, even, roll off to prevent high frequency noise amplification. This also helps to attenuate the feedback response of any unmodeled, high frequency modes. Due to these practical reasons against exact differentiation, the control system should implement the following position feedback

$$
\begin{aligned}
F_i(s) &= K_f K_a K_v \left(K_p (X_{com}(s) - X_i(s)) - \frac{Hs}{1+\beta s} X_i(s) \right) \\
&= K_f K_a K_p K_v \left(X_{com}(s) - \frac{1 + \left(\beta + \frac{H}{K_p}\right)s}{1+\beta s} X_i(s) \right) \\
&= K_f K_a K_c \left(X_{com}(s) - \frac{1+\alpha s}{1+\beta s} X_i(s) \right)
\end{aligned}
\tag{6-9}
$$

A continuous-time block diagram, that implements the feedback of Equation 6-9, is shown in Figure 6-3. In this block diagram, the position feedback and the modified velocity feedback are combined into one feedback path through a system with a lead transfer function where $\alpha > \beta$. The control system is designed such that α, β, and K_c produce two dominant closed-loop poles. This system will, therefore, behave very much like a second order system; yet, it will not be too sensitive to unmodeled high frequency modes or to high frequency noise on the position feedback signal.

The block diagram in Figure 6-3 is a continuous-time model of a system that is actually implemented as a discrete-time, digital control system. The continuous-time model has been used to simplify the current control system presentation. The block diagram of Figure 6-3 can be transformed into a discrete-time control system model in order to accurately represent the actual feed drive system. The new control system block diagram uses discrete-time equivalent transfer functions for the elements of the transfer matrix given in Equation 6-7. These discrete-time equivalent transfer functions can be obtained from

$$G_{i,j}(z) = \left(\frac{z-1}{z}\right) Z\left\{ L^{-1}[G_{i,j}(s)]\Big|_{t=kT} \right\} \tag{6-10}$$

where:

T = discrete-time sampling period
k = sampling index
Z = Z-transform operator
L^{-1} = Inverse Laplace Transform operator

The input to the servo amplifier comes from a digital-to-analog converter with a zero-order hold output. If the servo amplifier has a much wider bandwidth than the control

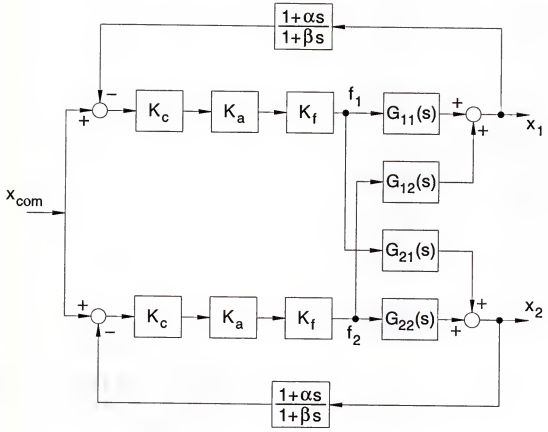

Figure 6-3. Block diagram of a continuous-time, dual, linear servomotor feed drive system with practical position feedback.

system bandwidth, then the linear motor force can be modeled as the output of a zero-order hold device. In this case, the transfer functions, given by Equation 6-10, exactly describe the samples of the rotor positions when the rotor forces are updated at discrete sampling instants. The lead, feedback compensation system can be mapped to a discrete-time transfer function using the bilinear transform [15]. Since the sampling frequency (4.5 kHz) for this digital control system is approximately 20 times greater than the control bandwidth, this emulation design technique will yield a discrete-time model that is close to the continuous-time model.

With a discrete-time model of the dual servomotor axis it is possible to accurately simulate the motion of the axis. The position loop control parameters α, β, and K_c are tuned to provide a position loop control bandwidth of 100 Hz and a damping ratio for the dominant closed-loop poles of 0.7 when the Y axis table is located in the center of the X axis saddle. The control system implementation shown in Figure 6-3 will achieve this performance if the control gain, K_c, is chosen such that $K_c K_a K_f$ = 1.58e8 N/m and the lead feedback compensation parameters are assigned the values α = 2.25e-3 s and β = 8.0e-5 s. The model is then modified to place the table is in the extreme top position to investigate the position loop response of both servomotors to a typical high-speed milling motion. Figure 6-4 shows the position loop frequency response from the discrete-time model for both motors when the table is in the extreme top position. The high frequency mismatch suggests that yaw errors will be evident during wide bandwidth operation of this drive. The axis performance is simulated with a command to move 100 mm at 30 m/min feedrate using triangular acceleration profiles having 1.0 g (g = 9.81 m/s^2) average acceleration, as shown in Figure 6-5. A 150 kg part is assumed to be attached to the table at a position that

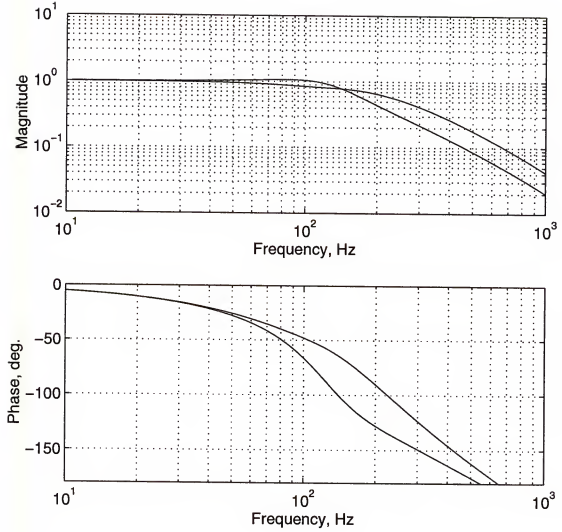

Figure 6-4. Position loop frequency response for both linear motors with the table is in the extreme top position.

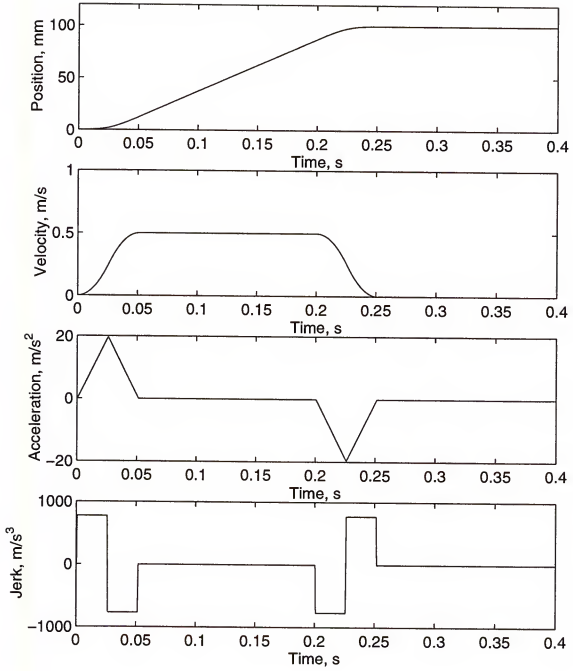

Figure 6-5. Axis motion command using 30 m/min feedrate and 1.0 g average acceleration with a triangular acceleration profile.

is 400 mm from the center of the saddle for this response simulation. The simulation program for this motion is written in the MATLAB programming language and is included in Appendix B. The axis yaw error reaches peak values of 34 μm/m during this motion as shown in Figure 6-6. This undesirable yaw error results from the unbalanced inertial loads that appear on the two independent position loops.

Yaw Error Reduction Through Coupled Servomotor Control

A machine axis with two or more motors that have parallel and separated lines of action lying in a plane that is parallel to the guideway plane can produce a resultant force that does not cause a yaw moment about the center of mass of the table. There are several approaches to achieving the desired motor forces. One method is to model the table mass distribution and then to modify the control loop tuning to compensate for the axis mass center location. This could be performed as an adaptive strategy for an axis with a time-varying mass distribution. Of course, this approach is only as effective as the accuracy of the model. A good model of this system could be difficult to identify, particularly in the case of compounded axes or for an axis which carries a changing workpiece mass.

An alternative approach to reducing the yaw errors resulting from the motor force is to apply feedback control to regulate against yaw rotation, while simultaneously controlling the axis position. This creates a coupled, two variable, position control system for one axis. The input to this control system is the desired position for the two servomotors. The position feedback comes from the rotor positions or from the saddle position at two widely separated locations. The axis yaw is measured from the difference between these two positions. This method uses feedback control to reduce the yaw errors in the axis motion without relying on accurate modeling of the axis mass distribution. A

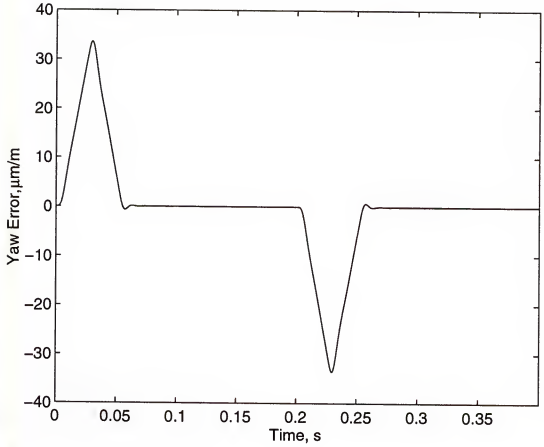

Figure 6-6. Axis yaw error under 30 m/min feedrate and 1.0 g average acceleration command as shown in Figure 6-5.

primary reason for applying feedback control is to accurately control systems with time-varying models or model uncertainties. Therefore, this approach is considered to be the most desirable solution since it can offer robustness to model uncertainties. Additionally, this control strategy does not require any additional hardware to implement beyond what is required for the IPLC system. Since the desired yaw motion is ideally zero, the yaw error control task is actually a regulation problem. Therefore, this control system will be referred to as the yaw regulation position control (YRPC) system.

The coupled control of the two servomotors on the X axis saddle can be viewed as a control system that drives the center of the saddle to track the axis position command while it simultaneously regulates against yaw errors on the axis. This viewpoint leads to a natural change in feedback parameters as suggested in the following coordinate transformation

$$\begin{bmatrix} x_c \\ x_d \end{bmatrix} = \begin{bmatrix} \frac{1}{2} & \frac{1}{2} \\ -1 & 1 \end{bmatrix} \begin{bmatrix} x_1 \\ x_2 \end{bmatrix} = T \begin{bmatrix} x_1 \\ x_2 \end{bmatrix} \tag{6-11}$$

where:

$$T = \begin{bmatrix} \frac{1}{2} & \frac{1}{2} \\ -1 & 1 \end{bmatrix} = \text{coordinate transformation matrix}$$

x_c = position of axis center

x_d = difference in position across axis

The axis center coordinate, x_c, defines the position of the center of the saddle as the average value of the two rotor positions. The position difference coordinate, x_d, defines the difference in the rotor positions which is approximately proportional to the yaw angle

for small rotation angles. The displacement coordinates x_1 and x_2 will be referred to as the rotor coordinates while the new displacements x_c and x_d will be referred to as the yaw coordinates.

The corresponding linear motor force transformation is given by

$$\begin{bmatrix} f_1 \\ f_2 \end{bmatrix} = \begin{bmatrix} \frac{1}{2} & -1 \\ \frac{1}{2} & 1 \end{bmatrix} \begin{bmatrix} f_c \\ f_d \end{bmatrix} = T^T \begin{bmatrix} f_c \\ f_d \end{bmatrix} \tag{6-12}$$

where f_c and f_d are the motor forces in the transformed yaw coordinate system.

A new transfer matrix can be defined in the yaw coordinate system by using the coordinate transformation given in Equation 6-11 and using the transfer matrix equation from Equation 6-7 in the rotor coordinates.

Then, the displacements can be related to the forces in the yaw coordinate system by

$$\begin{bmatrix} x_c \\ x_d \end{bmatrix} = T \begin{bmatrix} G_{1,1}(s) & G_{1,2}(s) \\ G_{2,1}(s) & G_{2,2}(s) \end{bmatrix} T^T \begin{bmatrix} f_c \\ f_d \end{bmatrix} = \begin{bmatrix} G_{c,c}(s) & G_{c,d}(s) \\ G_{d,c}(s) & G_{d,d}(s) \end{bmatrix} \begin{bmatrix} f_c \\ f_d \end{bmatrix} \tag{6-13}$$

where:

$$G_{c,c}(s) = \frac{2\left[(m_s + m_t)\left(\frac{y_c}{w_b}\right)^2 + \frac{J_c}{w_b^2}\right]s^2 + \left(\frac{w_g}{w_b}\right)^2 c_g s + \left(\frac{w_g}{w_b}\right)^2 k_g}{(m_s + m_t)\left[2\frac{J_c}{w_b^2}s^2 + \left(\frac{w_g}{w_b}\right)^2 c_g s + \left(\frac{w_g}{w_b}\right)^2 k_g\right]s^2} \tag{6-14}$$

$$G_{c,d}(s) = G_{d,c}(s) = \frac{2\frac{y_c}{w_b}}{2\frac{J_c}{w_b^2}s^2 + \left(\frac{w_g}{w_b}\right)^2 c_g s + \left(\frac{w_g}{w_b}\right)^2 k_g} \tag{6-15}$$

$$G_{d,d}(s) = \frac{2}{2\frac{J_c}{w_b^2}s^2 + \left(\frac{w_g}{w_b}\right)^2 c_g s + \left(\frac{w_g}{w_b}\right)^2 k_g} \tag{6-16}$$

In the yaw coordinate system, the cross transfer function terms, given by Equation 6-15, are proportional to the mass center location, y_c. When the table is located in the center of the saddle, the center of mass for the saddle and table system will be equal to zero and the cross transfer function terms will then be equal to zero. In this case, the transfer matrix in the yaw coordinates, given by Equation 6-13, is diagonal.

$$\begin{bmatrix} x_c \\ x_d \end{bmatrix} = \begin{bmatrix} \frac{1}{(m_s + m_t)s^2} & 0 \\ 0 & \frac{2}{2\frac{J_c}{w_b^2}s^2 + \left(\frac{w_g}{w_b}\right)^2 c_g s + \left(\frac{w_g}{w_b}\right)^2 k_g} \end{bmatrix} \begin{bmatrix} f_c \\ f_d \end{bmatrix} \tag{6-17}$$

When the axis is in this symmetrical configuration, the translational dynamics are uncoupled from the rotational dynamics. The control system design is simplified in this configuration since the problem reduces to two single-input, single-output (SISO) control systems. One SISO system controls the position of the axis center while the other SISO system controls the axis yaw motion. It is true that the yaw control loop is unnecessary in the symmetrical configuration in which it is designed. In fact, the independent position control loops previously discussed will also move the axis without yaw errors when the table is centered on the saddle. The benefit of the yaw control system is realized when the table is moved away from the saddle center position. In this configuration, the transfer matrix of Equation 6-13 is no longer diagonal and the control system variables are coupled. If the dynamic coupling is not too great, the control system which was designed

for the uncoupled system will be effective at regulating the yaw errors while simultaneously driving the center of the table to follow the axis command.

Design of the Yaw Error Control System

When the table of the compounded Y axis is located in the center of the X axis saddle, the translational and rotational dynamics become uncoupled, as seen in Equation 6-17. The control system design is performed with the Y axis in this position since the two variable control system can be separated into two single-input, single-output control systems in this configuration. One feedback control system controls the X axis center position while the other axis controls the yaw error for the axis. It is assumed that the control system will remain effective and stable when the Y axis table position changes and the two control loops become coupled. The control of the center position of X axis saddle is the same as a standard positional servomotor system. The block diagram for this uncoupled control system appears as shown in Figure 6-7. The model parameters m_s and m_t are the mass of the saddle and the mass of the table, respectively. The gain K_c is the proportional gain for the position control loop. The block gains K_a and K_f are the servo amplifier gain and linear motor force constants, respectively. The parameter α of the lead feedback system provides the necessary control loop damping while the parameter β limits high frequency noise from being fed back from the output. If the controller gain K_c is chosen such that $K_c K_a K_f$ = 3.16e8 N/m and the lead feedback network is designed such that α = 2.23e-3 s and β = 8.0e-5 s, then the control of the saddle center position will have a 100 Hz bandwidth and damping ratio of 0.7 for the dominant closed-loop poles. This position loop control system specification will ensure that the center of the saddle

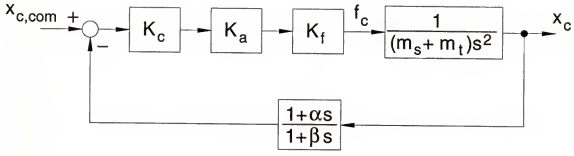

Figure 6-7. Position loop block diagram for the X axis saddle center position when Y axis table is symmetrically located with respect to the X axis saddle.

accurately tracks the wide bandwidth axis commands necessary for high-speed milling. The control system of Figure 6-7 generates the control system force f_c which produces equal motor forces f_1 and f_2, as can be seen in Equation 6-12. It should be emphasized that this control loop only feeds back the axis center position. Therefore, this control loop will tolerate any amount of yaw position error without creating a restoring moment between the two linear motors. The yaw position error will only be limited by the guideway stiffness. However, this amount of yaw error may not be satisfactory.

A second feedback control system is necessary to control the yaw rotation error on the X axis. This control system takes the difference in the linear rotor positions, x_d, as the feedback signal and generates a force difference, f_d, for the two linear motors. This difference in motor forces creates a yaw moment that attempts to minimize the yaw error on the axis. This control system is also designed for the symmetrical cross axis configuration that uncouples the translational and yaw motions of the X axis. The transfer function that describes the yaw response of the X axis saddle, $G_{d,d}(s)$, is given by Equation 6-16. This transfer function represents a single degree-of-freedom spring and mass vibration system. The natural frequency, ω_{ny}, and damping ratio, ζ_y, for this yaw mode of vibration are given by

$$\omega_{ny} = w_g\sqrt{\frac{k_g}{2J_c}} \tag{6-18}$$

$$\zeta_y = \frac{w_g c_g}{\sqrt{k_g J_c}} \tag{6-19}$$

Using the parameter values specified in Table 6-2, the yaw mode natural frequency is ω_{ny} = 335 rad/s (53 Hz) and the damping ratio is ζ_y = 0.067.

Since the yaw transfer function has a lowpass character, it is appropriate to consider a controller with one integrator to give a strong low frequency performance. However, an integral gain alone would only be stable for small closed-loop bandwidths. This stability limitation results from attempting to design a control system with three open-loop poles without any stabilizing open-loop zeros. To stabilize the system for wide bandwidth operation, the position difference feedback signal can be processed by a second order lead compensation. The yaw error control system block diagram is shown in Figure 6-8 for the symmetrical configuration of the compounded axes. This control system contains a reference input that could be used to control the yaw position of the saddle. This might be useful for small corrections in yaw error along the axis motion. It will be assumed, for this work, that the command input, $x_{d,com}$, is zero for all time, and thus the control system performs regulation of the axis yaw error. The usefulness of this regulator, control loop is realized when the Y axis moves away from the center of the X axis saddle, and the block diagrams shown in Figures 6-7 and 6-8 become coupled through the cross transfer functions $G_{cd}(s) = G_{dc}(s)$ as given by Equation 6-15.

The design of the yaw control system can be accomplished by first assuming that $\omega_c = \infty$ for the second order lead term. This reduces the control system design to a third order system with three parameters K_i, ω_d, and ζ_d. Since there are three design variables, it is possible that all three closed-loop poles can be specified. A possible choice for the closed-loop pole locations is to specify the third order Butterworth lowpass filter pole locations. If K_i is chosen such that $K_i K_a K_f = 6.3e10$ and $\omega_d = 447$ rad/s and $\zeta_d = 0.63$, then the closed-loop poles will match the pole locations for a third order Butterworth lowpass filter with a 100 Hz cutoff frequency. If the lead compensation is then changed such that

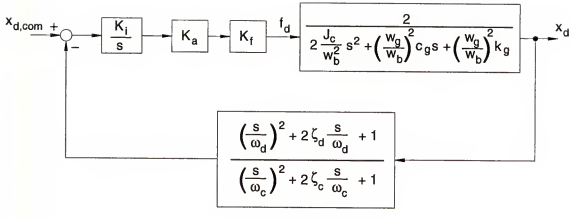

Figure 6-8. Yaw control loop block diagram for the X axis saddle when Y axis table is symmetrically located with respect to the X axis saddle.

ω_c = 15.7e3 rad/s and ζ_c = 0.7 which limits the high frequency gain, then the dominant closed-loop poles will remain nearly the same as for the third order Butterworth lowpass filter. Limiting the high frequency gain provides an increased margin of stability against unmodeled, high frequency modes and also attenuates any high frequency noise on the feedback signal.

A block diagram of the combined position loop control system and the yaw error control system is shown in Figure 6-9. This diagram shows the structural coupling that exists between the two control loops. The block diagram shows that the position loop input command, $x_{c,com}$, controls the position of center of the saddle, x_c, as is desired. It is also apparent that the position command, $x_{c,com}$, generates a control force, f_c, which will also tend to produce a yaw motion, x_d, on the saddle whenever $G_{dc}(s) \neq 0$. The goal of the yaw error control system design is minimize the closed-loop transfer function between the yaw error, x_d, and the axis command, $x_{c,com}$.

As was done for the IPLC system, the modeling and control system design has been performed for a continuous-time model of the YRPC system. This is justified by having a small loop closing time for the control system in order that emulation control design techniques can be applied. The frequency response computations and the simulations which will be subsequently presented are all based on discrete-time control models with a 221 μs loop closing time. These discrete-time models are obtained by using the discrete equivalent transfer function formula given by Equation 6-10 on each of the elements of the transfer matrix defined by Equation 6-13. The transfer functions for the control system compensation are converted to discrete-time transfer functions using the bilinear transform.

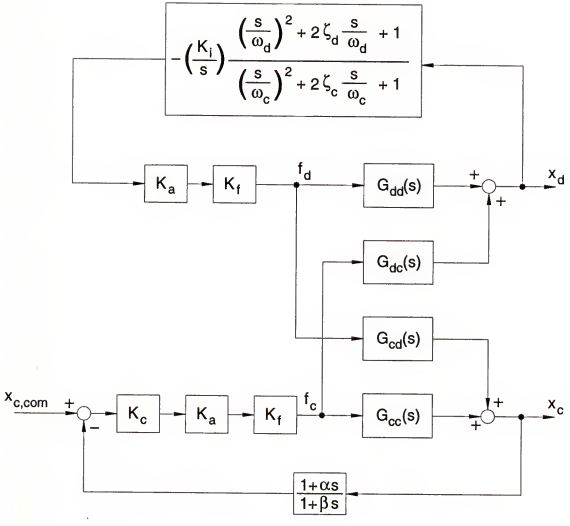

Figure 6-9. Combined position loop and yaw error control system.

The frequency response of the position control loop for the discrete-time model of the YRPC system is shown in Figure 6-10 for the configuration where the cross axis table is in the center of the saddle. In this axis arrangement, the mass center and the yaw error control loops are uncoupled. The position loop for this configuration clearly shows a bandwidth of 100 Hz. When the cross axis table is moved to the extreme top position, which is assumed to be 400 mm above the saddle center, the control system becomes coupled between the center position, x_c, and the yaw motion, x_d. The position loop frequency response in this configuration is shown in Figure 6-11. It is seen to be only slightly different from the response shown in Figure 6-10 where the system symmetry uncouples the linear and rotational dynamics. The frequency response of the position loop is demonstrated to be satisfactory in the two extremes of position for the cross axis table. It is, therefore, assumed that the X axis performance will be acceptable throughout the range of motion of the Y axis table.

The other important measure of the YRPC system performance is the yaw response to applied axis motion commands. The effectiveness of this control system at reducing yaw errors can be interpreted from the frequency response between the yaw error, x_d, and the axis command, $x_{c,com}$. This frequency response is given Figure 6-12 for the axis configuration where the Y axis is in the extreme top position. Ideally, this response should be small over all frequencies within the bandwidth of the axis command. The yaw response magnitude is small at low frequencies and increases with frequency up to a maximum value near 100 Hz, which is the bandwidth of the yaw control loop. Above this peak in the yaw frequency response, the magnitude rolls off continuously with increasing frequency. The overall magnitude of this frequency response increases with the

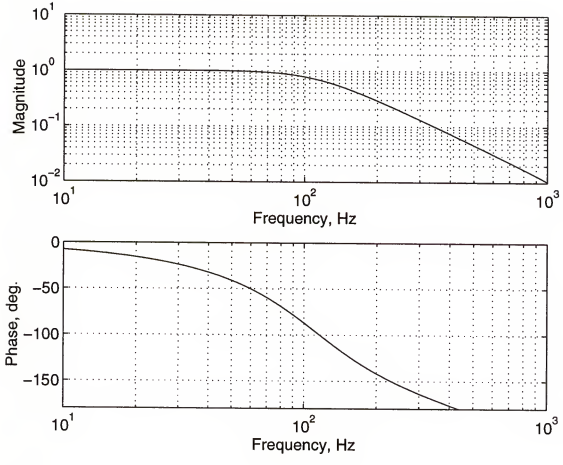

Figure 6-10. Axis position frequency response, $X_c(f)/X_{c,com}(f)$, for the yaw regulating axis control system when the cross axis table is in the center of the saddle.

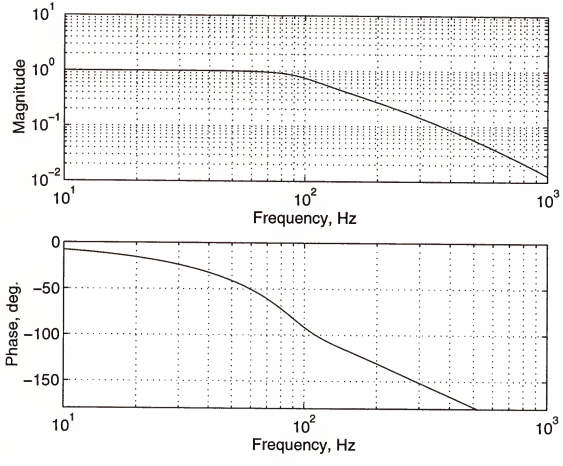

Figure 6-11. Axis position frequency response, $X_c(f)/X_{c,com}(f)$, for the yaw regulating axis control system when the cross axis table is in the extreme top position.

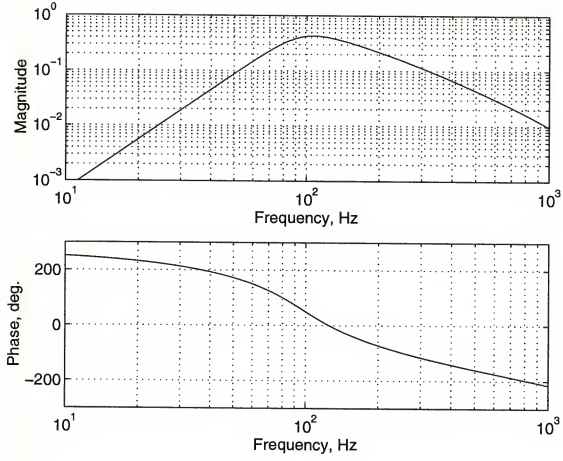

Figure 6-12. Axis yaw frequency response, $X_d(f)/X_{c,com}(f)$, for the yaw regulating axis control system when the cross axis table is in the extreme top position.

distance of the table from the center of the saddle and is equal to zero when the table is positioned in the center of the saddle.

A fundamental consideration for any control system is whether the system remains stable under all operating conditions. It is also important to determine the degree of relative stability of the control system to ensure that excessive oscillations do not arise from poorly damped system poles. The determination of relative stability for multivariable control systems can be somewhat complex to establish in general. However, since the control system used for the YRPC system is an uncoupled controller, it is practical to investigate stability using the technique of sequential loop closing. The system stability can be ascertained by first examining the stability of the yaw error control loop with the position control loop inactive. Once the yaw error control loop stability is assured, then the position loop stability can be analyzed under the condition that the yaw control loop is active.

The open-loop frequency response for the yaw error control loop, when the position control loop is inactive, is shown in Figure 6-13a for the axis configuration which places the table in the center of the saddle. Although this feedback control system is conditionally stable for smaller control system gains, it has good relative stability with 51 degrees of phase margin for the design gain. The open-loop frequency response for the yaw error control system when the table is in the extreme top position is displayed in Figure 6-13b. There is only a small decrease in the natural frequency of the yaw vibration mode without any significant difference in the relative stability of the control system. Therefore, this control loop should be robust to the possible changes in the Y axis position.

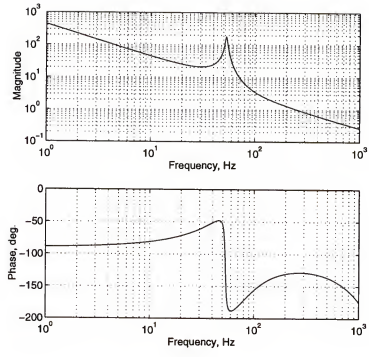

(a)

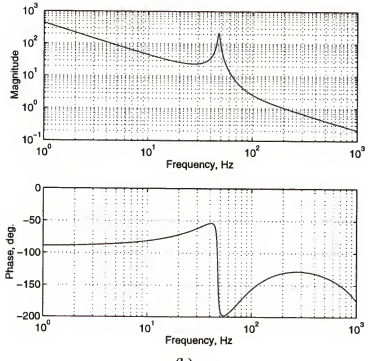

(b)

Figure 6-13. Open-loop frequency response for the yaw control loop with the position control loop inactive.
a) Y axis table in the center of saddle; b) Y axis table in the extreme top position.

With the stability of the yaw control loop assured, it is possible to analyze the stability of the coupled, two variable control system by analyzing the open-loop frequency response of the position control loop with the yaw control loop active. The open-loop frequency response for the position loop with the table in the center of the saddle is shown in Figure 6-14a. This control loop shows good relative stability with 55 degrees of phase margin. The same open-loop frequency response for the position loop when the table is in the extreme top position is shown in Figure 6-14b. This response shows the coupled effect of the yaw vibration mode due to the shift in the axis mass center. Although this mode creates an obvious change in the frequency response, it does not have an important effect on the control system stability. The relative stability of the YRPC system is not significantly altered from the design performance by placing the table in the extreme top position. Therefore, it is assumed that the entire control system will be insensitive to intermediate table positions and that it will remain effective for all locations of the table.

Simulated Motion Response of the Yaw Regulating Position Control System

The performance of the position control loop for the X axis saddle under the YRPC system may be evaluated by comparison with the IPLC system under identical motion commands. For all comparisons, the cross axis table on the Y axis will be assumed to be in the extreme top position which is 400 mm above the center of the X axis saddle. This should represent the worst case situation for the yaw error. The yaw error response for the IPLC system was previously presented in Figure 6-6 for the position command shown in Figure 6-5. The peak yaw error was found to be 34 μm/m for the IPLC system when both position loops were tuned for 100 Hz bandwidths.

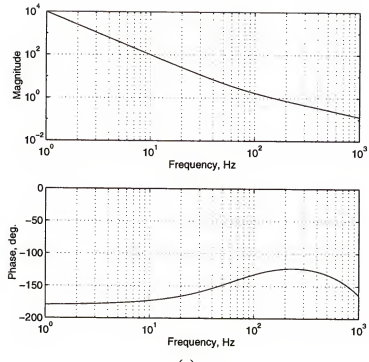

(a)

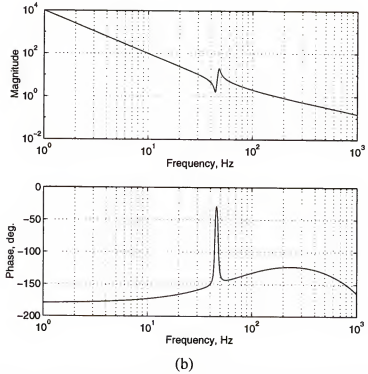

(b)

Figure 6-14. Open-loop frequency response for the position control loop with the yaw control loop active.
a) Y axis table in the center of saddle; b) Y axis table in the extreme top position.

The motion simulations are evaluated using a discrete-time model for the YRPC system. The yaw error, when the position command shown in Figure 6-5 is applied to the YRPC system, is shown in Figure 6-15. The peak yaw error is reduced to 2.7 μm/m for this system when the position control and yaw regulation loops are both tuned for 100 Hz bandwidths. The YRPC system shows a 12.5 times reduction in the yaw error compared with the IPLC system under identical axis motion commands. The program used for this motion simulation is included in Appendix B.

If further reduction of yaw errors is desired, this can be achieved by increasing the bandwidth of the yaw feedback control loop. If the yaw error control loop of the YRPC system is modified to have closed-loop dominant pole locations corresponding to a three pole Butterworth lowpass filter with a 150 Hz cutoff frequency, then the yaw error for the same position command is reduced to a peak value of 0.76 μm/m. The yaw error in response to this position command is shown in Figure 6-16. This improved YRPC system gives an additional 3.5 times reduction in the yaw error for a modest 50 percent increase in the control bandwidth of the yaw regulation control loop.

The modeling results presented in this chapter show that an order of magnitude reduction in the axis yaw errors during acceleration are realistically possible for axes with time-varying mass center location. The reduction in yaw error remains effective even under substantial changes in the axis mass center location. The control scheme requires that the axis have two, or more, independently controllable servomotors. Additionally, the servomotors must have separated lines of action in order to control the location of the resultant motor force. Axes that satisfy these servomotor requirements can be controlled against yaw rotation without any additional hardware expense.

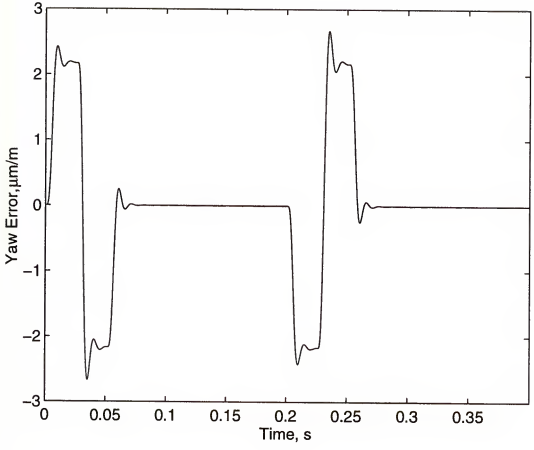

Figure 6-15. Yaw error for the yaw regulating position loop control system in response to the command with a triangular acceleration profile as shown in Figure 6-5.

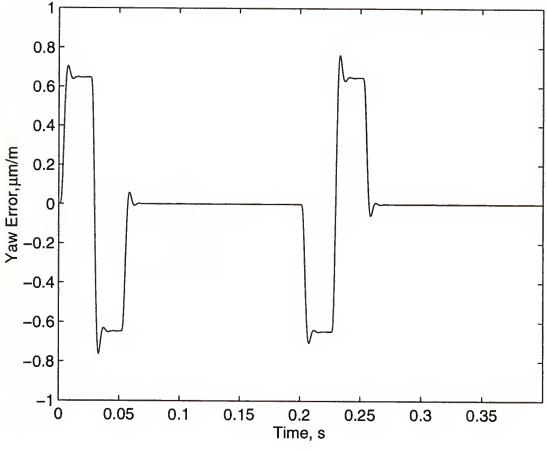

Figure 6-16. Yaw error for the improved yaw regulating position loop control system in response to the command with a triangular acceleration profile as shown in Figure 6-5.

CHAPTER 7
DELAY EQUALIZATION FOR MULTIPLE AXES

The performance of a machine tool axis is often characterized by the position loop bandwidth and by the maximum attainable acceleration and feedrate. Another common measure of axis performance is the positional following error in response to axis commands. These measures of axis performance are important since they determine how closely the axis will follow the command. However, on a multiple axis machine tool it is important to know not just how well an individual axis performs; but also, how well all of the axes operate together. This can be expressed by the tracking error, which is measured under multiple axis motions. The tracking error at any point in time, during a multiple axis motion, is defined as the distance between the actual axis position and the nearest point on the command path. A two axis motion command contour is shown in Figure 7-1. The coordinate of the position command and the actual position of the two axes at a given time during the motion is also indicated in this figure. The positional following errors for the X axis and the Y axis are identified as e_x and e_y respectively. The tracking error is also labeled in this figure as e_t. It is important to notice that the following errors can be rather large while the tracking error can be much smaller or can even be zero for certain commands.

It is frequently stated that gain mismatch between the axes of a machine tool leads to increased tracking errors [8]. If all of the axes on a machine tool are tuned identically,

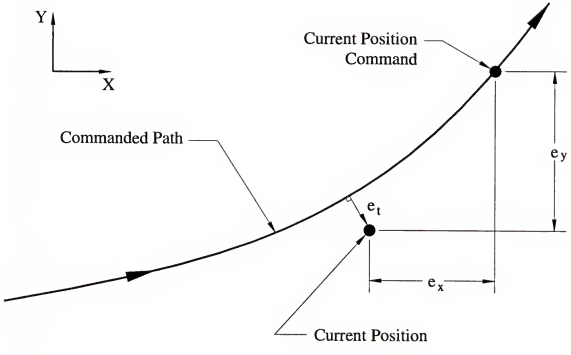

Figure 7-1. Illustration of multiple axis tracking error e_t.

then the tracking errors for certain commands will be minimal for a given control bandwidth. In practice, it is not always possible and it is not always necessary to have identical tuning for each axis. On a five-axis, high-speed milling machine, for example, it may be permissible for the rotational axes to have a smaller response bandwidth than the linear axes. If the bandwidths of the individual axis commands do not exceed the response bandwidths of each servomotor control loop, then each axis will follow its own command without attenuation. Although each axis may follow its command accurately, the tracking errors may be very large due to unequal phase delays associated with the different axis bandwidths.

Comparison of Tracking Errors for Unequal Bandwidth Axes

The tracking error under two axis motions can be easily investigated through simulation. This will be done for two linear axes in X and Y coordinates which have different position loop control bandwidths. It will be assumed that the X axis is the faster axis with a 100 Hz bandwidth while the Y axis is slower with a 25 Hz bandwidth. The axes are assumed to be well tuned in that the damping ratio is approximately 0.7 for both axes. The axes are modeled as in Chapter 6 where lead compensation of the position feedback signal is used. The discrete-time transfer functions, using a 221 μs sampling period, for the position loop response can be approximated by Equations 7-1 and 7-2 for the X axis and Y axis, respectively.

$$G_x(z) = 9.6395\times10^{-3}\frac{z+1}{z^2-1.79596z+0.815239} \tag{7-1}$$

$$G_y(z) = 6.0100\times10^{-4}\frac{z+1}{z^2-1.95080z+0.952002} \tag{7-2}$$

A two dimensional command path that can be used to investigate the two axis tracking error is shown in Figure 7-2. This motion simultaneously exercises both axes in order that tracking errors can occur. The motion starts at the axis origin with a constant 0.2 g acceleration to a 0.25 m/s feedrate. The feedrate is held constant at 0.25 m/s through the remainder of the motion including the 25 mm constant radius turn of 90 degrees. The actual path of the X and Y axes in also plotted along with the position command in Figure 7-2. It is clear that the tracking error is large for this two axis motion. The tracking error during the motion is shown in Figure 7-3 versus the motion time. The tracking error reaches a maximum of 850 μm during the motion. This amount of tracking error would be unacceptable for most milling operations. Therefore, some type of compensation must be applied to reduce the tracking error.

Feedforward Correction of Tracking Errors

Feedforward compensation of various forms can be utilized to reduce or eliminate the tracking errors associated with multiple axis motions when the servomotor control loops do not all have equal performance. Most of these compensation strategies design a feedforward system that has a transfer function which is the inverse of the position loop such that the overall axis performance ideally has an infinite response bandwidth. These methods include the standard velocity and acceleration feedforward compensations that are commonly implemented on commercial machine tool controllers. Also included in the infinite bandwidth class of feedforward controllers is the Zero Phase Error Tracking Control (ZPETC) system proposed by Tomizuka [9]. Some feedforward compensations only attempt to achieve equal bandwidths for all axes, which equalizes the performance for all axes on the machine. This strategy has been proposed by Weck [11] to avoid

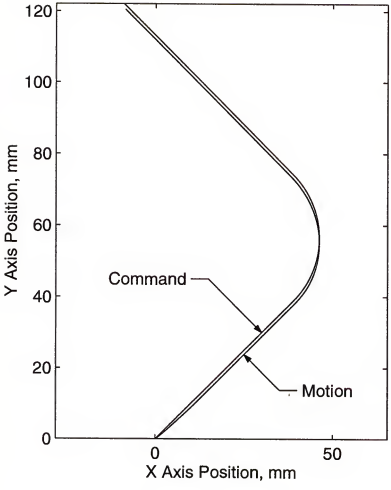

Figure 7-2. Two axis command contour and motion path using the servomotor transfer function models given in Equations 7-1 and 7-2.

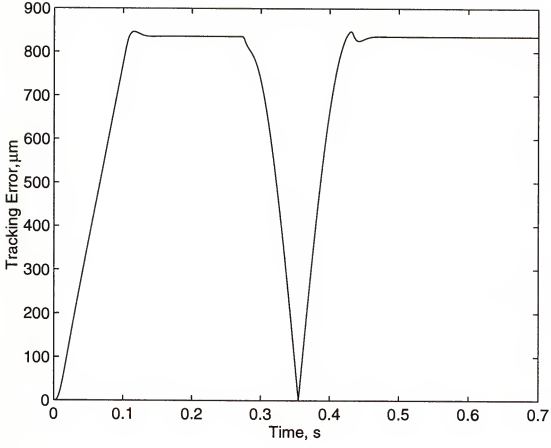

Figure 7-3. Tracking error for the two axis command in Figure 7-2 using the position loop transfer function models given by Equations 7-1 and 7-2.

problems of axis saturation. Additionally, increasing the bandwidth of an axis may amplify resonances in the drive structure which could cause undesirable tracking errors during transient motions.

For many machine tools it is unnecessary to increase the bandwidth of the slow axes. This is due to the fact that, for many commands, the tracking error results primarily from the difference in the phase delay between different axes. This will be true as long as the bandwidth of the position command for each axis does not exceed the position loop response bandwidth. For these commands, a feedforward compensation which equalizes the phase delay for each axis will be sufficient to achieve accurate tracking error performance.

Frequency Response Comparison for Axes with Different Bandwidths

Servomotor control systems for machine tools are almost always implemented on digital processors, therefore, the position loop can be most accurately described by a discrete-time transfer function. The procedure for modeling the discrete-time transfer function has been previously been shown in Chapter 5. To simplify the current presentation, the position loop for a well tuned axis with a fast position loop closing frequency can be approximately modeled by a continuous-time second order transfer function as given by

$$G_p(s) = \frac{\omega_n^2}{s^2 + 2\zeta\omega_n s + \omega_n^2} \tag{7-3}$$

where:

ω_n = position loop natural frequency

ζ = position loop damping ratio

The frequency response for the continuous-time transfer function of Equation 7-3 can be approximated by an ideal system

$$G_{pi}(\omega) = \begin{cases} e^{-j\omega T_d} & \text{for } \omega \le \omega_n \\ 0 & \text{for } \omega > \omega_n \end{cases} \approx G_p(\omega) \tag{7-4}$$

where:

$$T_d = \frac{2\zeta}{\omega_n} = \text{time delay constant}$$

The exact frequency response for the transfer function given by Equation 7-3 and the approximate frequency response of Equation 7-4 is shown in Figure 7-4 for a system with a 100 Hz natural frequency and a damping ratio of 0.7. The approximation is most accurate at low frequencies which is usually where most of the spectral content of the axis commands will be found.

The magnitude of the approximate frequency response function given by Equation 7-4 is unity for frequencies below ω_n. The phase for the frequency response function given by Equation 7-4 is

$$\angle G_{pi}(\omega) = \begin{cases} -\omega T_d & \text{for } \omega \le \omega_n \\ \text{undefined} & \text{for } \omega > \omega_n \end{cases} \tag{7-5}$$

The phase within the position loop bandwidth of this system model is linear with frequency. It is well known in the communications engineering field that systems that have linear phase and constant magnitude are capable of distortionless transmission with

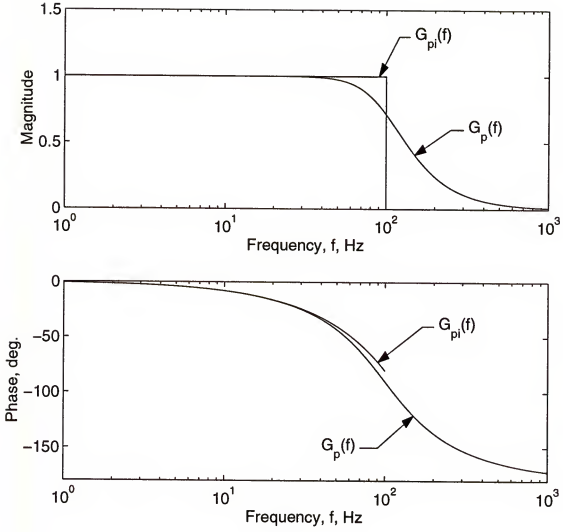

Figure 7-4. Frequency response comparison between Equation 7-3, $G_p(f)$, and Equation 7-4, $G_{pi}(f)$.

only a time delay between the input and output. This result will be exploited to reduce the tracking errors that exist between the axes with different bandwidths.

It will be assumed that the position command for each axis is bandlimited to the bandwidth, ω_n, of the axis feed drive. Then the Fourier transform of the command signal for the axis, $X_c(\omega)$, will be approximately equal to zero for frequencies greater than ω_n.

$$X_c(\omega) \approx 0 \qquad \text{for } \omega > \omega_n \tag{7-6}$$

The Fourier transform of the axis response, designated by $X_r(\omega)$, can then be represented by

$$X_r(\omega) = G_p(\omega)X_c(\omega) \approx G_{pi}(\omega)X_c(\omega) \approx e^{-j\omega T_d}X_c(\omega) \tag{7-7}$$

The inverse Fourier transform of Equation 7-7 is obtained by using the delay property of the Fourier transform.

$$x_r(t) \approx x_c(t - T_d) \tag{7-8}$$

The result indicates that the response will be approximately the same as the command signal except that it will be delayed in time relative to the command. It can be shown that the velocity error constant, K_v, for a system with the transfer function given by Equation 7-1 is

$$K_v = \frac{1}{T_d} = \frac{\omega_n}{2\zeta} \tag{7-9}$$

The steady-state position lag for a constant velocity input command is determined by dividing the velocity magnitude by the velocity error constant. Alternatively, if the axis is following a constant velocity command with purely a time delay of T_d, then the position lag must be equal to the product of the velocity magnitude and the time delay of the

system. The time delay property of linear phase systems is not just limited to steady-state operation but applies to much more general types of inputs. The only requirement on the input signal is that it must satisfy the bandwidth limitation given by Equation 7-6.

Based on the linear phase model of Equation 7-4, a machine tool which has axes with different bandwidths and similar damping ratios will execute motion commands with different time delays on the individual axes. Assuming all of the axes have nearly equal damping ratios, the axes that have a larger control bandwidth will execute motions with a smaller time delay. A difference in the axis time delays can result in substantial tracking errors during multiple axis motions since the individual axis motions will be unsynchronized.

The time delay parameter of the linear phase system model suggests a method for equalizing the delays on all of the machine axes. The correction strategy is to determine the time delay for each axis of the machine and then to delay the commands to the faster axes such that each axis will execute motion commands with the same time delay as the slowest axis. Since the delay is applied to the position loop command signal this will have no effect of the stability of the position control system. The time delay for each axis can be determined experimentally by commanding motions that satisfy Equation 7-6 to each axis and measuring the time delay of the response. Perhaps the simplest test that could be used to determine time delay for an axis is to measure the steady-state following error for a constant velocity motion. The steady-state positional lag divided by the commanded velocity would easily, and accurately, provide the measured time delay for an axis.

The time delay associated with the discrete-time transfer functions given by Equations 7-1 and 7-2 can be determined analytically or experimentally by simulating the

response to a constant velocity command. The X axis transfer function, with the 100 Hz position loop bandwidth, has a time delay of 2.228 ms while the Y axis, which has only a 25 Hz bandwidth, has a time delay of 8.912 ms. The smaller bandwidth Y axis is four times slower than the X axis for these axis models. If the command signal to the faster X axis is delayed by 6.684 ms then both axes will be in synchronization and the tracking errors will be dramatically reduced. The response to the motion command shown in Figure 7-2 can again be simulated with the equalizing time delay of 6.684 ms applied to the X axis command. The tracking error with the time delay compensation is shown in Figure 7-5. The maximum tracking error is now reduced to only 10.5 μm which is a reduction of more than 80 times compared with the uncompensated axes.

The delay compensation is a form of feedforward compensation since it modifies the command to the position loop. There are two approaches toward delaying the axis commands. The first method is to generate the delayed axis commands directly as part of the command generation process. This is the most straightforward solution but not necessarily the easiest to implement.

A second method for implementing delay compensation would be to be design a delay filter for undelayed axis commands. Since the positional servomotor is a digital control system it is easy to implement an accurate time delay. If the required delay for an axis is an integer multiple of the servomotor loop closing period then it is an easy process to delay the command by the proper number of samples. Achieving greater accuracy will usually require delaying the command by a non-integer number of samples. This involves interpolation of the command signal to obtain the proper time delay. A delay filter which

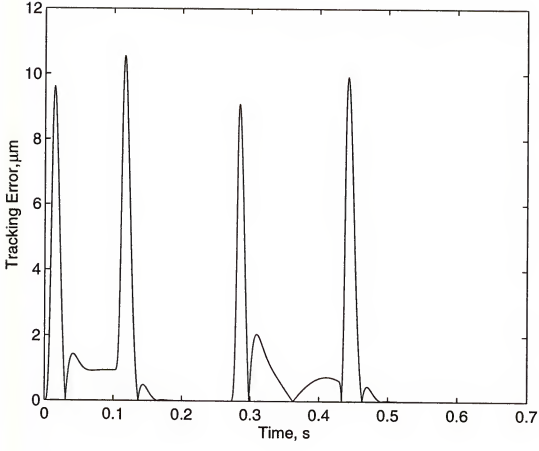

Figure 7-5. Tracking error for the two axis command in Figure 7-2 using the position loop transfer function models given by Equations 7-1 and 7-2 with delay equalization of 6.684 ms applied to the X axis.

requires a delay of N whole samples and a fraction α of a sample period can be constructed using linear interpolation as

$$x_d(k) = (1-\alpha)x_c(k-N) + \alpha x_c(k-(N+1)) \tag{7-10}$$

Higher order interpolation could be utilized if greater delay accuracy is required. The Z-transform of Equation 7-10 identifies the transfer function of the delay filter.

$$\frac{X_d(z)}{X_c(z)} = (1-\alpha)z^{-N} + \alpha z^{-(N+1)} \tag{7-11}$$

This is a finite impulse response filter which can be efficiently implemented on digital signal processing devices and requires very few processor operations per sample. Unfortunately, a delay filter such as this is not usually implemented on commercial machine tool controllers. Therefore, at the present time, this time delay equalization technique can only be implemented on truly open architecture controllers or on custom servomotor control hardware.

Phase Linearization

The phase portion of the frequency response plot shown in Figure 7-4 is replotted in Figure 7-6 with a linear frequency axis scaling to show the phase linearity for the continuous-time position loop model which is given by $G_p(\omega)$. The phase of the frequency response approximation, $G_{pi}(\omega)$, is strictly linear with respect to frequency. Although the position loop frequency response is quite linear, especially at low frequencies, there is a maximum phase difference between the two models of 9.8 degrees at the natural frequency of 100 Hz.

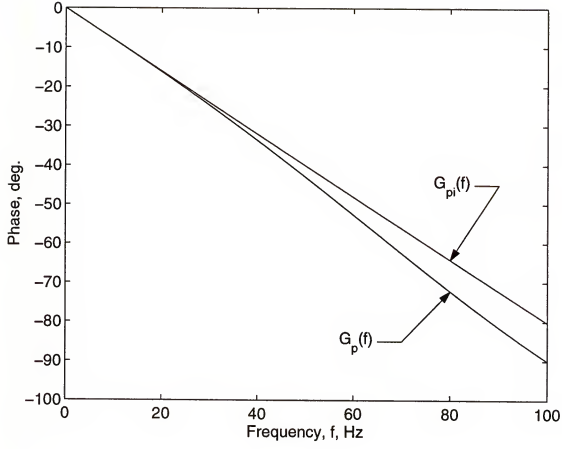

Figure 7-6. Frequency response phase comparison between Equation 7-3, $G_p(f)$, and Equation 7-4, $G_{pi}(f)$.

The small nonlinearity of the phase leads to phase distortions in the axis response. It is possible to add additional feedforward compensation to further linearize the system phase. Phase equalization is a well developed procedure for use in communications systems where the time delay of a signal is of little importance as long as the waveform is transmitted without distortion. This criteria suits the needs of machine tool control systems since it does not matter whether the part is machined a fraction of a second later as long as the part is manufactured with sufficient accuracy.

Phase equalization is usually accomplished using a cascade of transfer functions called allpass filters. These filters have the useful property of a constant frequency response magnitude for all frequencies and a phase which is nonlinear with frequency. The form of a discrete-time, second order, allpass transfer function is given by

$$G_{ap}(z) = \frac{a_2 z^2 + a_1 z + 1}{z^2 + a_1 z + a_2} \tag{7-12}$$

The zeros of this transfer function are located at the reciprocal of the pole locations with the poles located within the unit circle for stability. The design of these allpass systems for delay equalization of systems is somewhat complex and usually requires the use of nonlinear optimization algorithms [15].

The design procedure involves finding the proper allpass filter coefficients that minimize the variation of the group delay of the cascaded allpass systems combined with the position loop over all frequencies within the position loop bandwidth. The group delay of a transfer function is defined as the derivative with respect to frequency of the frequency response phase. If the group delay is constant then the phase will be linear. The group delay for the transfer functions given by Equations 7-1 and 7-2 are shown in

Figure 7-7. These are the transfer functions that are used for the two axis contour simulation shown in Figure 7-2. The group delay varies by approximately 22 percent over the position loop bandwidth for each axis.

The first step in the allpass filter design is to choose the filter order. Higher order filters may yield better group delay equalization but the filter order must be balanced against the computational effort required to execute the filters on the axis controller. It has been found that the systems with the group delays shown in Figure 7-7 can be effectively compensated with sixth order allpass filters. The design of the allpass filter coefficients is accomplished using nonlinear optimization techniques. One optimization algorithm that has been proven to work well for these allpass compensation designs has been proposed by Deczky [16]. This program is based on a modified version of the Fletcher-Powell constrained minimization algorithm. The optimization routine used for this work is also based on the Fletcher-Powell algorithm and is available in the MATLAB Optimization toolbox.

The optimization criteria applied to this filter design minimizes the peak-to-peak variation of the group delay over the position loop bandwidth. The poles are constrained to have magnitudes less than one to maintain stable filter designs. The sixth order allpass equalization filters that were designed using this approach are given by Equation 7-13 for the X axis and by Equation 7-14 for the Y axis.

$$G_{apx}(z) = \left(\frac{0.8360z^2-1.7933z+1}{z^2-1.7933z+0.8360}\right)\left(\frac{0.7201z^2-1.6972z+1}{z^2-1.6972z+0.7201}\right)\left(\frac{0.2402z^2-0.9565z+1}{z^2-0.9565z+0.2402}\right) \tag{7-13}$$

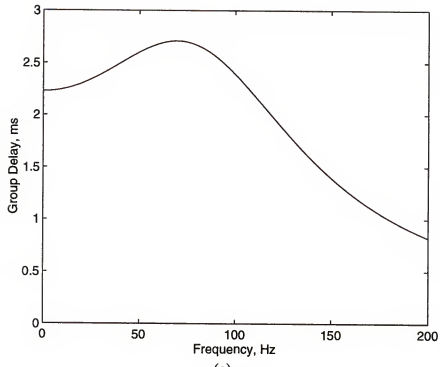

(a)

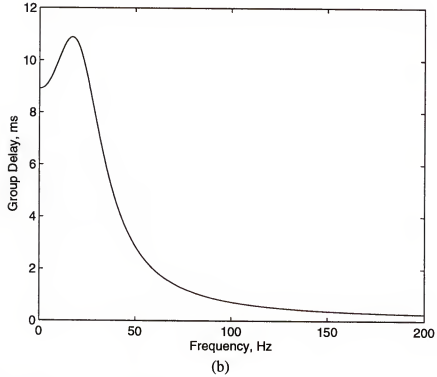

(b)

Figure 7-7. Position loop group delay.
a) X axis group delay; b) Y axis group delay.

$$G_{apy}(z) = \left(\frac{0.9559z^2-1.9530z+1}{z^2-1.9530z+0.9559}\right)\left(\frac{0.9213z^2-1.9197z+1}{z^2-1.9197z+0.9213}\right)\left(\frac{0.7071z^2-1.6798z+1}{z^2-1.6798z+0.7071}\right)$$

(7-14)

A MATLAB program that was used to design the allpass compensation filters $G_{apx}(z)$ and $G_{apy}(z)$ is included in Appendix C. The equalized group delay for the X axis and for the Y axis is shown in Figure 7-8. The group delays with the allpass equalization are substantially larger than the group delays for the uncompensated axes. The group delay variation over the bandwidth of both axes is now significantly reduced compared to the group delay variation without the allpass compensation. This will reduce the phase distortions associated with the nonlinear phase of the axis servomotor at the higher frequencies within the control bandwidth. The X axis command requires an additional constant time delay of 31.50 ms to match the time delay of the Y axis.

To establish the improvement gained though phase equalization with the allpass compensation, the same position command contour that was shown in Figure 7-2 can be simulated again with the allpass phase equalization and the new time delay for the X axis applied. The resulting tracking error is presented in Figure 7-9. The maximum tracking error is now reduced to a maximum of only 5.3 μm. This is represents a 159 times improvement compared with tracking error of the uncompensated axes. Although, the improvement is only 2.0 times better than the performance obtained by simply delaying the command to the faster X axis servomotor without any allpass phase compensation.

The compensation based only on delaying the command to the faster axis provides excellent tracking error reduction. It is also simple to tune and efficient to implement on a DSP based controller. Therefore, this feedforward compensation should be considered as

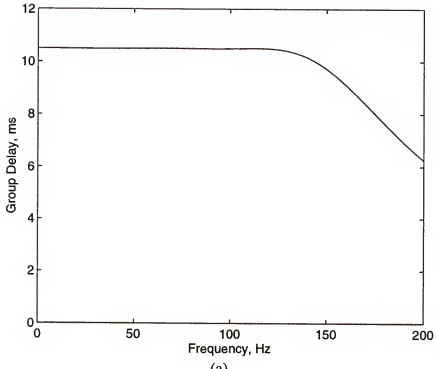

(a)

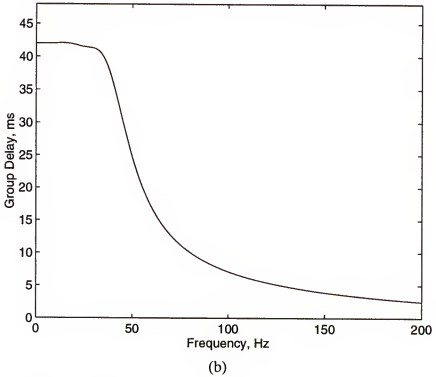

(b)

Figure 7-8. Allpass equalized position loop group delay.
a) X axis equalized group delay; b) Y axis equalized group delay.

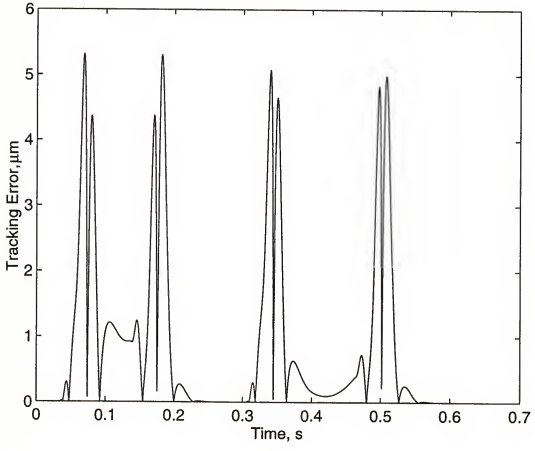

Figure 7-9. Tracking error for the two axis command in Figure 7-2 using the position loop transfer function models given by Equations 7-1 and 7-2 with allpass phase equalization applied.

an alternative to other methods which result in increased axis bandwidth since this may not be required or may not even be beneficial. By comparison, the allpass phase equalization compensation does provide improved tracking performance, although at a considerable expense of design time and processing power to implement. Therefore, it seems that the complexity of this compensation may not be justified for many applications. However, the allpass compensation may provide greater tracking error reduction for certain motion commands. Especially, commands with greater frequency content near, but within, the bandwidth of the slower axis.

CHAPTER 8
CONCLUSIONS AND RECOMMENDATIONS

High-speed milling machines demand high-performance machine tool feed drives in order to fully benefit from high spindle speeds. It has been shown that it is essential to design high-speed milling machine feed drives with up to 40 m/min axis feedrates, 2 g accelerations and position loop control bandwidths of at least 100 Hz. The research to date has not adequately addressed the control issues related to wide bandwidth feed drive operation. The design of feed drive control systems for wide bandwidth applications usually requires special control system compensation for structural vibration modes that may exist in the feed drive components. Without proper compensation, control system instability may result or the axes may suffer from excessive tracking error.

The X and Y axes of the MTRC high-speed milling machine use conventional feed drive designs with recirculating ballscrew transmissions. These drives have two important torsional vibration modes that can lead to control system instability without proper compensation. The feed drive control system was stabilized for wide bandwidth control using a pole and zero canceling compensator for the structural modes. This control strategy achieved a closed position loop control bandwidth of 100 Hz with 2 g accelerations and 30 m/min feedrates. There are additional vibration modes associated with this drive design that are external to the position control loop when feedback is returned from a rotary encoder. These modes can result in dynamic position errors under wide bandwidth axis commands. Feedforward compensation could potentially be used to

compensate for these modes but the dynamics of these modes vary with the saddle and table positions as well as the workpiece mass. This makes feedforward compensation a challenging task that may require adaptive modification. The use of linear position scales on these axes would include these modes within the control system which may create stability problems. Additional research is needed to contend with the problems this configuration would create.

The use of linear motors for high-speed milling machine feed drives eliminates the ballscrew transmission and the associated structural dynamics. The linear drive technology usually permits increased position loop control bandwidth. There are also additional benefits of using linear motors for high-speed milling machines such as increased service life at high feedrates and accelerations. However, the trade-off is a more expensive drive with much greater sensitivity to the table mass. Additionally, structural dynamics associated with the axis table and guideways may lead to similar control system stability concerns as were encountered with the conventional ballscrew design.

The use of multiple motors with separated lines of action on a single axis allows the simultaneous control of the axis position and regulation against axis rotation errors. This is beneficial when the axis mass distribution is unequal with respect to each motor. A model of the compounded X and Y axes on the MTRC machine with linear motor feed drives has been created to study the effect of yaw regulated axis control of the X axis saddle. Simulation results indicate that yaw errors can be reduced by an order of magnitude, or more, compared with independent position loop control of separated motors. This performance improvement can be achieved without additional cost since it does not require any additional hardware beyond what is required for independent position

loop control. This type of axis control is not currently implemented by any known axis controllers; therefore, it must be implemented on open architecture or custom control systems.

It has been shown that wide bandwidth servomotor control is necessary for high-speed milling machines. However, it may not be practical, or even be necessary, to achieve wide bandwidth control on every axis of a high-speed milling machine. This might be the case on five-axis machine tools where the rotational axes may be limited to smaller control bandwidths. It is important, though, that all of the axes on the machine tool perform well together in order that tracking errors will be minimized. Assuming that all axes of the machine tool have sufficient bandwidth to follow the individual axis commands, then accurate motion tracking can be achieved by time delay equalization of the axis commands. This requires that the commands to the fast axes are properly delayed in such a manner that all axes will be in the proper positions at the same time. Simulations of delay equalization techniques indicate that tracking error reductions on the order of 100 times are possible for axes with a bandwidth ratio of 4:1.

The simplest delay equalization technique considered requires that the position commands to the fast axes be delayed by a constant time delay. The required time delay can be rapidly, and accurately, measured for each individual axis from the steady-state following error to constant velocity motion commands. This tuning procedure is considerably simpler than other feedforward compensation techniques. In fact, the tuning procedure can easily be automated. Some methods, such the ZPETC feedforward compensation, require complete system identification for accurate tuning.

Delay equalization using a pure time delay as a feedforward compensation can be easily implemented on a digital signal processor and would require very few instructions per servo cycle. This time delay type of feedforward compensation is not currently supported by major servomotor controller manufacturers. Therefore, implementation of this compensation technique will be restricted to open architecture and custom servomotor controllers. In spite of the lack of commercial support for this feedforward compensation, this technique is very powerful and can provide substantial tracking error reduction for a machine tool with mismatched tuning between axes.

APPENDIX A
FINITE ELEMENT MODEL OF BALLSCREW FEED DRIVE

```
% ____________________________________________________________
%
% MATLAB Finite element model of the MTRC high-speed milling
% machine ballscrew feed drive
% ____________________________________________________________

% material properties
E=200e9;
nu=0.27;
rho=7850;

% model parameters
NumBallElm=25;
NumCoupElm=5;
NumRotorElm=10;
dof = 2*(NumBallElm+NumCoupElm+NumRotorElm+3)+1;

% store node numbers for each element
BallElm=[1:NumBallElm]';
CoupElm=max(BallElm)+[1:NumCoupElm]';
RotorElm=max(CoupElm)+[1:NumRotorElm]';

BallNodes=[1:NumBallElm+1]';
CoupNodes=max(BallNodes)+[1:NumCoupElm+1]';
RotorNodes=max(CoupNodes)+[1:NumRotorElm+1]';

ElmNodes=[[min(BallNodes):max(BallNodes)-1]', ...
          [min(BallNodes)+1:max(BallNodes)]'; ...
          [min(CoupNodes):max(CoupNodes)-1]', ...
          [min(CoupNodes)+1:max(CoupNodes)]'; ...
          [min(RotorNodes):max(RotorNodes)-1]', ...
          [min(RotorNodes)+1:max(RotorNodes)]'];

K=zeros(dof);
M=zeros(dof);

LBall=1.35;
LCoup=0.082;
LRotor=0.305;
DoBall=0.056;
DiBall=0.011;
DoCoup=0.090;
DiCoup=0.0773;
DoRotor=0.0773;
DiRotor=0.0;
```

```
% Coupling stiffness
kCpA = 1e5;
kCpT = 5e6;

% tapered roller bearing stiffness
kTRB = 4e9;

% motor ball bearing stiffness
kBB = 1e6;

% ballnut parameters
kBN=3.6e7;        % ballnut thrust stiffness
xBN=0.5*LBall;    % location of ballnut

% table parameters
r = 0.02/(2*pi);
mt = 225;

% Assemble the ballscrew elements
lBall=LBall/NumBallElm;
x=lBall*[0:NumBallElm]';
kel=ElStiff(lBall,DiBall,DoBall-0.006,E,nu);
mel=ElMass(lBall,DiBall,DoBall,rho);
for i=1:NumBallElm
 rows=[2*(ElmNodes(BallElm(i),1)-1)+ ...
       1:2*(ElmNodes(BallElm(i),2)-1)+2];
 cols=rows;
 K = AddElement(K,kel,rows,cols);
 M = AddElement(M,mel,rows,cols);
end

% Assemble the coupling elements
lCoup=LCoup/NumCoupElm;
x=[x;LBall+lCoup*[0:NumCoupElm]'];
kel=ElStiff(lCoup,DiCoup,DoCoup,E,nu);
mel=ElMass(lCoup,DiCoup,DoCoup,rho);
for i=1:NumCoupElm
 rows=[2*(ElmNodes(CoupElm(i),1)-1)+ ...
       1:2*(ElmNodes(CoupElm(i),2)-1)+2];
 cols=rows;
 K = AddElement(K,kel,rows,cols);
 M = AddElement(M,mel,rows,cols);
end

% Assemble the rotor elements
lRotor=LRotor/NumRotorElm;
```

```
x=[x;LBall+LCoup+lRotor*[0:NumRotorElm]'];
kel=ElStiff(lRotor,DiRotor,DoRotor-0.030,E,nu);
mel=ElMass(lRotor,DiRotor,DoRotor,rho);
for i=1:NumRotorElm
 rows=[2*(ElmNodes(RotorElm(i),1)-1)+ ...
       1:2*(ElmNodes(RotorElm(i),2)-1)+2];
 cols=rows;
 K = AddElement(K,kel,rows,cols);
 M = AddElement(M,mel,rows,cols);
end

% couple the ballscrew and rotor with the coupling torsional
stiffness
kelCoup=[kCpA, 0, -kCpA, 0; 0, kCpT, 0, -kCpT; ...
        -kCpA, 0, kCpA, 0; 0, -kCpT, 0, kCpT];

rows=[2*(ElmNodes(BallElm(NumBallElm),2)-1)+ ...
      1:2*(ElmNodes(CoupElm(1),1)-1)+2];
cols=rows;
K = AddElement(K,kelCoup,rows,cols);

rows=[2*(ElmNodes(CoupElm(NumCoupElm),2)-1)+ ...
      1:2*(ElmNodes(RotorElm(1),1)-1)+2];
cols=rows;
K = AddElement(K,kelCoup,rows,cols);

% apply thrust stiffness from tapered roller bearing
kelTRB=[kTRB, 0; 0 0];
rows=[2*(ElmNodes(BallElm(NumBallElm),1)-1)+ ...
      1:2*(ElmNodes(BallElm(NumBallElm),1)-1)+2];
cols=rows;
K = AddElement(K,kelTRB,rows,cols);

% apply thrust stiffness from rotor ball bearing
kelBB=[kBB, 0; 0 0];
rows=[2*(ElmNodes(RotorElm(1),2)-1)+ ...
      1:2*(ElmNodes(RotorElm(1),2)-1)+2];
cols=rows;
K = AddElement(K,kelBB,rows,cols);

% Add table to the model
M(dof,dof) = mt;
kelBN = kBN*[1, -r, -1; -r, r^2, r; -1, r, 1];
NutNode = min(NumBallElm, ...
 max(0,round((xBN/LBall)*NumBallElm))) + 1;
rows = [2*(NutNode-1)+1,2*(NutNode-1)+2,dof];
```

```
cols=rows;
K = AddElement(K,kelBN,rows,cols);

% eigen solution
[P,Lam] = eig(K,M);
P=real(P);
Lam=real(Lam);
wn=diag(Lam).^0.5;

% sort the eigen solution from lowest eigenvalue to highest
[wn,order]=sort(wn);
P=P(:,order);
Lam=Lam(:,order);
fn=wn/(2*pi);

% scale eigenvectors so that maximum element is 1
[PbigLin,iLin]=max(abs(P(1:2:dof,:)));
[PbigRot,iRot]=max(abs(P(2:2:dof-1,:)));

for i=1:length(wn)
 if ( PbigLin(i) > r*PbigRot(i) )
  scale(i) = P(2*iLin(i)-1,i)/r;
 else
  scale(i) = P(2*iRot(i),i);
 end
end
P=P*diag(1.0./scale);

% Calculate torsional modal stiffness between rotation at
% the free end of rotor where the tach is attached and a
% uniformly distributed torque across the rotor.
Coord1=2*RotorNodes;
Coord2=2*max(RotorNodes);
Kd = P'*K*P;
Md = P'*M*P;
Kmodal = diag(Kd)./[mean(P(Coord1,:)).*P(Coord2,:)]';
Kmodal(1)=0;

% Plot lowest modeshapes
xMark=[LBall,LBall,LBall+LCoup,LBall+LCoup];
yMark=[-1,1,1,-1];

for i=1:20
 figure(i)
 subplot(2,1,1)
 y=P(1:2:dof-1,i);
```

```
 plot(x,y,xMark,r*yMark,x(NutNode),P(dof,i),'r+')
 limits=axis;
 axis([limits(1:2),-r,r])
 title(sprintf('Modeshape %1.1f Hz, ...
  k = %1.2e Nm/rad',fn(i), Kmodal(i)))
 ylabel('Axial')
 subplot(2,1,2)
 y=P(2:2:dof-1,i);
 plot(x,y,xMark,yMark)
 limits=axis;
 axis([limits(1:2),-1,1])
 ylabel('Torsional')
end

% plot frequency response between the rotor and the
% tachometer
zeta=0.01*ones(length(fn),1);% emperical damping ratios
zeta(3)=0.05;

f=logspace(1,4,1000)';
G=-mean(P(Coord1,1)).*P(Coord2,1)./(Md(1,1)*(2*pi*f).^2);

for i=[3,5,7]
 G = G + ...
 1.0./(Kmodal(i)*(1-(f/fn(i)).^2 + j*2*zeta(i)*(f/fn(i))));
end
G=j*2*pi*f.*G;   % convert to velocity response

% plot frequency response
figure(gcf+1)
subplot(2,1,1);
loglog(f,abs(G))
grid
xlabel('Frequency, Hz');
ylabel('Magnitude, (rad/s)/Nm');
subplot(2,1,2);
semilogx(f,unwrap(angle(G))*180/pi)
grid
xlabel('Frequency, Hz');
ylabel('Phase, deg.');
print 'BallscrewFEAFR' -deps
```

```
% ____________________________________________________________
%
% Matlab function to generate the element stiffness matrix
% ____________________________________________________________

function kel=ElStiff(l,di,do,E,nu)

A=pi*(do^2-di^2)/4;
J=pi*(do^4-di^4)/32;
G=E/(2*(1+nu));

kel=(1/l)*[ E*A,     0,  -E*A,     0 ; ...
               0,   G*J,     0,  -G*J ; ...
            -E*A,     0,   E*A,     0 ; ...
               0,  -G*J,     0,   G*J ];


% ____________________________________________________________
%
% Matlab function to generate the element mass matrix
% ____________________________________________________________

function mel=ElMass(l,di,do,rho)

A=pi*(do^2-di^2)/4;
J=pi*(do^4-di^4)/32;

mel = (rho*l/6)*[2*A,    0,    A,    0 ; ...
                   0,  2*J,    0,    J ; ...
                   A,    0,  2*A,    0 ; ...
                   0,    J,    0,  2*J ];
```

APPENDIX B
YAW ERROR CONTROL SYSTEM PROGRAMS

```
% ____________________________________________________________
%
% MATLAB program to simulate axis motion using the
% Independent Loop Position Control (ILPC) system
% ____________________________________________________________

% model parameters
yt=0.4;
ms=450;
mt=350;
as=0.530;
bs=1.525;
at=0.710;
bt=0.710;
wb=0.790;
wg=0.375;
kg=200e6;
cg=28300;
Ts=221e-6;

Kp=1.58e8;
alpha=2.25e-3;
beta=8.0e-5;

yc=mt*yt/(ms+mt);
Js=ms*(as*as+bs*bs)/12;
Jt=mt*(at*at+bt*bt)/12;
Jc=Js+ms*yc^2+Jt+mt*(yt-yc)^2;

% discrete equivalent transfer functions
ratio=(wg/wb)^2;
n11s=[0.5*(ms+mt)*(2*yc/wb-
1)^2+2*Jc/wb^2,ratio*cg,ratio*kg];
d11s=(ms+mt)*[2*Jc/wb^2,ratio*cg,ratio*kg,0,0];
G11=c2d(tf(n11s,d11s),Ts,'zoh');
[n11,d11]=tfdata(G11,'v');

n12s=[0.5*(ms+mt)*(2*yc/wb-
1)*(2*yc/wb+1)+2*Jc/wb^2,ratio*cg,ratio*kg];
d12s=(ms+mt)*[2*Jc/wb^2,ratio*cg,ratio*kg,0,0];
G12=c2d(tf(n12s,d12s),Ts,'zoh');
[n12,d12]=tfdata(G12,'v');

n21s=[0.5*(ms+mt)*(2*yc/wb+1)*(2*yc/wb-
1)+2*Jc/wb^2,ratio*cg,ratio*kg];
d21s=(ms+mt)*[2*Jc/wb^2,ratio*cg,ratio*kg,0,0];
```

```
G21=c2d(tf(n21s,d21s),Ts,'zoh');
[n21,d21]=tfdata(G21,'v');

n22s=[0.5*(ms+mt)*(2*yc/wb+1)^2+2*Jc/wb^2, ...
      ratio*cg,ratio*kg];
d22s=(ms+mt)*[2*Jc/wb^2,ratio*cg,ratio*kg,0,0];
G22=c2d(tf(n22s,d22s),Ts,'zoh');
[n22,d22]=tfdata(G22,'v');

% position control loop compensation
ngpc=Kp;
dgpc=1;
[nhpc,dhpc]=bilinear([alpha,1],[beta,1],1/Ts);

% Generate position command
g=9.81;
p=0.1;
v=0.5;
a=g;            % average acceleration
t=[0:Ts:0.4]';

AccelType = 2;
if AccelType == 1
 % constant jerk acceleration profile
 k=inf;
 [xcom, Tj, Ta, Tv, Tp]=trapazoidmotion(p,v,a,k,t);
elseif AccelType == 2
 % constant jerk acceleration profile
 ap=2*a;
 k=ap^2/v;
 [xcom, Tj, Ta, Tv, Tp]=trapazoidmotion(p,v,ap,k,t);
end

% Simulate the response to the command signal
[f1(1,1),zf1]=filter(ngpc,dgpc,xcom(1));
[f2(1,1),zf2]=filter(ngpc,dgpc,xcom(1));
[x11,zx11]=filter(n11,d11,f1(1));
[x12,zx12]=filter(n12,d12,f2(1));
[x21,zx21]=filter(n21,d21,f1(1));
[x22,zx22]=filter(n22,d22,f2(1));
x1(1,1)=x11+x12;
x2(1,1)=x22+x21;
[xfb1,zxfb1]=filter(nhpc,dhpc,x1(1));
[xfb2,zxfb2]=filter(nhpc,dhpc,x2(1));

for i=2:length(xcom)
```

```
 [f1(i,1),zf1]=filter(ngpc,dgpc,xcom(i)-xfb1,zf1);
 [f2(i,1),zf2]=filter(ngpc,dgpc,xcom(i)-xfb2,zf2);
 [x11,zx11]=filter(n11,d11,f1(i),zx11);
 [x12,zx12]=filter(n12,d12,f2(i),zx12);
 [x21,zx21]=filter(n21,d21,f1(i),zx21);
 [x22,zx22]=filter(n22,d22,f2(i),zx22);
 x1(i,1)=x11+x12;
 x2(i,1)=x22+x21;
 [xfb1,zxfb1]=filter(nhpc,dhpc,x1(i),zxfb1);
 [xfb2,zxfb2]=filter(nhpc,dhpc,x2(i),zxfb2);
end

figure(1)
plot(t,1e3*[xcom,x1,x2]);
xlabel('Time, s')
ylabel('Position, mm')

figure(2)
plot(t,1e6*(x2-x1))
axis([0,t(length(t)),-40,40])
xlabel('Time, s')
ylabel('Yaw Error, \mum/m')
print IndependYawErr2 -deps


% ____________________________________________________________
%
% MATLAB program to simulate axis motion using the
% Yaw Regulation Position Control (YRPC) system
% ____________________________________________________________

% model parameters
yt=0.4;
ms=450;
mt=350;
as=21*0.0254; %0.530;
bs=60*0.0254; %1.525;
at=27*0.0254; %0.710;
bt=27*0.0254; %0.710;
wb=31*0.0254; %0.790;
wg=14.75*0.0254; 0.375;
kg=200e6;
cg=28300;
Ts=221e-6;

Kp=3.16e8;
```

```
alpha=2.23e-3;
beta=8.0e-5;

YawBandwidth=1;
if YawBandwidth == 1
 Ki=6.3e10;
 wd=447;
 zetad=0.63;
elseif YawBandwidth == 2
 Ki=2.116e11;
 wd=669;
 zetad=0.67;
end
wc=15.7e3;
zetac=0.7;

yc=mt*yt/(ms+mt);
Js=ms*(as*as+bs*bs)/12;
Jt=mt*(at*at+bt*bt)/12;
Jc=Js+ms*yc^2+Jt+mt*(yt-yc)^2;

% discrete equivalent transfer functions
ratio=(wg/wb)^2;
nccs=[2*((ms+mt)*(yc/wb)^2+Jc/wb^2),ratio*cg,ratio*kg];
dccs=(ms+mt)*[2*Jc/wb^2,ratio*cg,ratio*kg,0,0];
Gcc=c2d(tf(nccs,dccs),Ts,'zoh');
[ncc,dcc]=tfdata(Gcc,'v');

ncds=2*yc/wb;
dcds=[2*Jc/wb^2,ratio*cg,ratio*kg];
Gcd=c2d(tf(ncds,dcds),Ts,'zoh');
[ncd,dcd]=tfdata(Gcd,'v');

ndcs=2*yc/wb;
ddcs=[2*Jc/wb^2,ratio*cg,ratio*kg];
Gdc=c2d(tf(ndcs,ddcs),Ts,'zoh');
[ndc,ddc]=tfdata(Gdc,'v');

ndds=2;
ddds=[2*Jc/wb^2,ratio*cg,ratio*kg];
Gdd=c2d(tf(ndds,ddds),Ts,'zoh');
[ndd,ddd]=tfdata(Gdd,'v');

% position control loop compensation
ngpc=Kp;
dgpc=1;
```

```
[nhpc,dhpc]=bilinear([alpha,1],[beta,1],1/Ts);

% yaw control loop feedback compensation
[ngyc,dgyc]=bilinear(Ki,[1,0],1/Ts);
[nhyc,dhyc]=bilinear([1/wd^2,2*zetad/wd,1], ...
                     [1/wc^2,2*zetac/wc,1],1/Ts);

% Generate position command
g=9.81;
p=0.1;
v=0.5;
a=g;           % average acceleration
t=[0:Ts:0.4]';

AccelType = 2;
if AccelType == 1
 % constant jerk acceleration profile
 k=inf;
 [xcom, Tj, Ta, Tv, Tp]=trapazoidmotion(p,v,a,k,t);
elseif AccelType == 2
 % constant jerk acceleration profile
 ap=2*a;
 k=ap^2/v;
 [xcom, Tj, Ta, Tv, Tp]=trapazoidmotion(p,v,ap,k,t);
end

% Simulate the response to the command signal
[fc(1,1),zfc]=filter(ngpc,dgpc,xcom(1));
[fd(1,1),zfd]=filter(ngyc,dgyc,0);
[xcc,zxcc]=filter(ncc,dcc,fc(1));
[xcd,zxcd]=filter(ncd,dcd,fd(1));
[xdc,zxdc]=filter(ndc,ddc,fc(1));
[xdd,zxdd]=filter(ndd,ddd,fd(1));
xc(1,1)=xcc+xcd;
xd(1,1)=xdd+xdc;
[xfbc,zxfbc]=filter(nhpc,dhpc,xc(1));
[xfbd,zxfbd]=filter(nhyc,dhyc,xd(1));

for i=2:length(xcom)
 [fc(i,1),zfc]=filter(ngpc,dgpc,xcom(i)-xfbc,zfc);
 [fd(i,1),zfd]=filter(ngyc,dgyc,-xfbd,zfd);
 [xcc,zxcc]=filter(ncc,dcc,fc(i),zxcc);
 [xcd,zxcd]=filter(ncd,dcd,fd(i),zxcd);
 [xdc,zxdc]=filter(ndc,ddc,fc(i),zxdc);
 [xdd,zxdd]=filter(ndd,ddd,fd(i),zxdd);
 xc(i,1)=xcc+xcd;
```

```
 xd(i,1)=xdd+xdc;
 [xfbc,zxfbc]=filter(nhpc,dhpc,xc(i),zxfbc);
 [xfbd,zxfbd]=filter(nhyc,dhyc,xd(i),zxfbd);
end

figure(1)
plot(t,1e3*[xcom,xc]);
xlabel('Time, s')
ylabel('Position, mm')

figure(2)
plot(t,1e6*xd)
xlabel('Time, s')
ylabel('Yaw Error, \mum/m')

if YawBandwidth == 1
 axis([0,t(length(t)),-3,3])
 print CoupledYawErr2a -deps
else
 axis([0,t(length(t)),-1,1])
 print CoupledYawErr2b -deps
end


% ____________________________________________________________
%
% MATLAB function to generate a position motion
% using trapazoidal acceleration profiles
% ____________________________________________________________

function [cmd, Tj, Ta, Tv, Tp]=trapazoidmotion(p,v,a,k,t)

% [cmd, Tj, Ta, Tv, Tp]=trapazoidmotion(p,v,a,k,t)
%
% Generate motion command using a constant jerk profile
%
% Inputs:
%  p - movement distance
%  v - maximum velocity
%  a - maximum acceleration
%  k - constant jerk may be inf (infinity)
%  t - vector of sample times
%
% Outputs:
%  cmd - motion command
%  Tj  - constant jerk phase duration
```

```
%  Ta  - constant acceleration phase duration
%  Tv  - constant velocity phase duration
%  Tp  - complete motion time Tp = 4*Tj + 2*Ta + Tv
%
%
% Written by: David A. Smith 11/98


Tj=a/k;
Ta=v/a-a/k;
Tv=p/v-v/a-a/k;
Tp=4*Tj+2*Ta+Tv;

p0=0;
v0=0;
a0=0;
cmd=0;

% const. jerk
if (k<inf)
 index=find(t<Tj);
 cmd=[cmd;k*(t(index).^3)/6];
 p0=k*(Tj^3)/6;
 v0=k*(Tj^2)/2;
end
a0=a;

% const. accel
index=find((Tj<t) & (t<=Tj+Ta));
tau=Tj;
cmd=[cmd;p0+v0*(t(index)-tau)+a0*((t(index)-tau).^2)/2];
p0=p0+v0*Ta+a0*(Ta^2)/2;
v0=v0+a0*Ta;
a0=a;

% const. jerk
if (k<inf)
 index=find((Tj+Ta<t) & (t<=2*Tj+Ta));
 tau=Tj+Ta;
 cmd=[cmd;p0+v0*(t(index)-tau)+ ...
      a0*((t(index)-tau).^2)/2-k*((t(index)-tau).^3)/6];
 p0=p0+v0*Tj+a0*(Tj^2)/2-k*(Tj^3)/6;
 v0=v0+a0*Tj-k*(Tj^2)/2;
end
a0=0;
```

```
% const. velocity
index=find((2*Tj+Ta<t) & (t<=2*Tj+Ta+Tv));
tau=2*Tj+Ta;
cmd=[cmd;p0+v0*(t(index)-tau)];
p0=p0+v0*Tv;
v0=v0;
a0=0;

% const. jerk
if (k<inf)
 index=find((2*Tj+Ta+Tv<t) & (t<=3*Tj+Ta+Tv));
 tau=2*Tj+Ta+Tv;
 cmd=[cmd;p0+v0*(t(index)-tau)+ ...
      a0*((t(index)-tau).^2)/2-k*((t(index)-tau).^3)/6];
 p0=p0+v0*Tj+a0*(Tj^2)/2-k*(Tj^3)/6;
 v0=v0+a0*Tj-k*(Tj^2)/2;
end
a0=-a;

% const. accel
index=find((3*Tj+Ta+Tv<t) & (t<=3*Tj+2*Ta+Tv));
tau=3*Tj+Ta+Tv;
cmd=[cmd;p0+v0*(t(index)-tau)+a0*((t(index)-tau).^2)/2];
p0=p0+v0*Ta+a0*(Ta^2)/2;
v0=v0+a0*Ta;
a0=-a;

% const. jerk
if (k<inf)
 index=find((3*Tj+2*Ta+Tv<t) & (t<=4*Tj+2*Ta+Tv));
 tau=3*Tj+2*Ta+Tv;
 cmd=[cmd;p0+v0*(t(index)-tau)+ ...
      a0*((t(index)-tau).^2)/2+k*((t(index)-tau).^3)/6];
 p0=p0+v0*Tj+a0*(Tj^2)/2+k*(Tj^3)/6;
 v0=v0+a0*Tj+k*(Tj^2)/2;
end
a0=0;

% const. position
cmd=[cmd;p0*ones(length(t)-length(cmd),1)];
```

```
% ____________________________________________________________
%
% MATLAB program to analyze the stability of the
% Yaw Regulation Position Control (YRPC) system
% ____________________________________________________________

% model parameters
yt=[0,0.4];
ms=450;
mt=350;
as=21*0.0254; %0.530;
bs=60*0.0254; %1.525;
at=27*0.0254; %0.710;
bt=27*0.0254; %0.710;
wb=31*0.0254; %0.790;
wg=14.75*0.0254; 0.375;
kg=200e6;
cg=28300;
Ts=221e-6;

Kp=3.16e8;
alpha=2.23e-3;
beta=8.0e-5;

YawBandwidth=1;
if YawBandwidth == 1
 Ki=6.3e10;
 wd=447;
 zetad=0.63;
elseif YawBandwidth == 2
 Ki=2.116e11;
 wd=669;
 zetad=0.67;
end
wc=15.7e3;
zetac=0.7;

for i=1:length(yt)
 yc=mt*yt(i)/(ms+mt);
 Js=ms*(as*as+bs*bs)/12;
 Jt=mt*(at*at+bt*bt)/12;
 Jc=Js+ms*yc^2+Jt+mt*(yt(i)-yc)^2;
 f=logspace(0,3,1000)';

 % discrete equivalent transfer functions
 ratio=(wg/wb)^2;
```

```
nccs=[2*((ms+mt)*(yc/wb)^2+Jc/wb^2),ratio*cg,ratio*kg];
dccs=(ms+mt)*[2*Jc/wb^2,ratio*cg,ratio*kg,0,0];
[ncc,dcc]=tfdata(c2d(tf(nccs,dccs),Ts,'zoh'),'v');
Gcc=freqz(ncc,dcc,2*pi*f*Ts);

ncds=2*yc/wb;
dcds=[2*Jc/wb^2,ratio*cg,ratio*kg];
[ncd,dcd]=tfdata(c2d(tf(ncds,dcds),Ts,'zoh'),'v');
Gcd=freqz(ncd,dcd,2*pi*f*Ts);

ndcs=2*yc/wb;
ddcs=[2*Jc/wb^2,ratio*cg,ratio*kg];
[ndc,ddc]=tfdata(c2d(tf(ndcs,ddcs),Ts,'zoh'),'v');
Gdc=freqz(ndc,ddc,2*pi*f*Ts);

ndds=2;
ddds=[2*Jc/wb^2,ratio*cg,ratio*kg];
[ndd,ddd]=tfdata(c2d(tf(ndds,ddds),Ts,'zoh'),'v');
Gdd=freqz(ndd,ddd,2*pi*f*Ts);

% position control loop compensation
ngpc=Kp;
dgpc=1;
Gpc=freqz(ngpc,dgpc,2*pi*f*Ts);
[nhpc,dhpc]=bilinear([alpha,1],[beta,1],1/Ts);
Hpc=freqz(nhpc,dhpc,2*pi*f*Ts);

% yaw control loop feedback compensation
[ngyc,dgyc]=bilinear(Ki,[1,0],1/Ts);
Gyc=freqz(ngyc,dgyc,2*pi*f*Ts);
[nhyc,dhyc]=bilinear([1/wd^2,2*zetad/wd,1],...
                     [1/wc^2,2*zetac/wc,1],1/Ts);
Hyc=freqz(nhyc,dhyc,2*pi*f*Ts);

% Sequential loop closing
% Yaw control open loop frequency response
GHy(:,i)=Gyc.*Gdd.*Hyc;
[minval,iwg]=min(abs(1-abs(GHy(:,i))));
Phimy(i)=180+angle(GHy(iwg,i))*180/pi;

% Position control open loop
GHp(:,i)=Gpc.*(Gcc+Gdc.*Gcd./(1+GHy(:,i))).*Hpc;
[minval,iwg]=min(abs(1-abs(GHp(:,i))));
Phimp(i)=180+angle(GHp(iwg,i))*180/pi;
end
```

```
figure(1)
subplot(2,1,1);
loglog(f,abs(GHy(:,1)));
axis([1,1000,0.1,1000])
grid
xlabel('Frequency, Hz')
ylabel('Magnitude')
subplot(2,1,2)
semilogx(f,unwrap(angle(GHy(:,1)))*180/pi)
axis([1,1000,-200,0])
grid
xlabel('Frequency, Hz')
ylabel('Phase, deg.')
print YawOpenFrNoPosSym -deps

figure(2)
subplot(2,1,1);
loglog(f,abs(GHy(:,2)));
axis([1,1000,0.1,1000])
grid
xlabel('Frequency, Hz')
ylabel('Magnitude')
subplot(2,1,2)
semilogx(f,unwrap(angle(GHy(:,2)))*180/pi)
axis([1,1000,-200,0])
grid
xlabel('Frequency, Hz')
ylabel('Phase, deg.')
print YawOpenFrNoPos -deps

figure(3)
subplot(2,1,1);
loglog(f,abs(GHp(:,1)));
axis([1,1000,1e-2,1e4])
grid
xlabel('Frequency, Hz')
ylabel('Magnitude')
subplot(2,1,2)
semilogx(f,unwrap(angle(GHp(:,1)))*180/pi)
axis([1,1000,-200,0])
grid
xlabel('Frequency, Hz')
ylabel('Phase, deg.')
print PosOpenFrYawClosedSym -deps

figure(4)
```

```
subplot(2,1,1);
loglog(f,abs(GHp(:,2)));
axis([1,1000,1e-2,1e4])
grid
xlabel('Frequency, Hz')
ylabel('Magnitude')
subplot(2,1,2)
semilogx(f,unwrap(angle(GHp(:,2)))*180/pi)
axis([1,1000,-200,0])
grid
xlabel('Frequency, Hz')
ylabel('Phase, deg.')
print PosOpenFrYawClosed -deps
```

APPENDIX C
ALLPASS PHASE EQUALIZATION PROGRAMS

```
% ____________________________________________________________
%
% Allpass phase equalization program
% Equalizes the group delay for a servomotor position
%  control loop
% ____________________________________________________________

global fopt
global Tdpopt
global Ts

f=linspace(0.1,1000,1000)';

% discrete-time control system models
Ts=221e-6;
m=400;
wn=2*pi*100;
zeta=0.7;

K=m*wn.^2;
alpha=2*zeta/wn;
beta=2/(2*pi*1e8);

ng=0.5*K/m*(Ts^2)*[0,1,1];
dg=[1,-2,1];
nh=[2*alpha+Ts,-(2*alpha-Ts)];
dh=[2*beta+Ts,-(2*beta-Ts)];
Gp=feedback(tf(ng,dg),tf(nh,dh));
[np,dp]=tfdata(Gp,'v');

Gpf=freqz(np,dp,2*pi*f*Ts);
Tdp=-filter([1,-1],1,unwrap(angle(Gpf)))./ ...
     filter([1,-1],1,(2*pi*f));

% allpass design
flim=120;
var0=[0.8472,0.0027,0.49,0.22,0.9138,0.1989];
fopt=linspace(1,flim,50)';
Gpfopt=freqz(np,dp,2*pi*fopt*Ts);
Tdpopt=-filter([1,-1],1,unwrap(angle(Gpfopt)))./ ...
        filter([1,-1],1,(2*pi*fopt));

% minimization routine
options=foptions;
options(3)=1e-8;
var=constr('groupdelay',var0,options)
```

```
% extract allpass solution
order=length(var);
neq=1;
deq=1;
for sect=1:order/2
 r=var(2*sect-1);
 phi=var(2*sect);
 neq=conv(neq,[r^2,-2*r*cos(phi),1]);
 deq=conv(deq,[1,-2*r*cos(phi),r^2]);

 Geq=freqz(neq,deq,2*pi*f*Ts);
 Tde=-filter([1,-1],1,unwrap(angle(Geq)))./ ...
      filter([1,-1],1,(2*pi*f));
end

figure(1)
plot(f,1000*Tdp)
axis([0,200,0,3])
xlabel('Frequency, Hz')
ylabel('Group Delay, ms');

figure(gcf+1)
plot(f,1000*[Tde(:,1)])
axis([0,200,0,10])
xlabel('Frequency, Hz')
ylabel('Group Delay, ms');

figure(gcf+1)
plot(f,1000*[Tdp(:,1)+Tde(:,1)])
axis([0,200,0,12])
xlabel('Frequency, Hz')
ylabel('Group Delay, ms');
```

```
% Optimation function for allpass design
% Returns the peak to peak variation of
%  the equalized group delay

function [Err,G]=groupdelay(x)

global fopt
global Tdpopt
global Ts
order=length(x);

b=1;
a=1;
for i=1:order/2
 r=x(2*i-1);
 phi=x(2*i);

 b=conv(b,[r^2,-2*r*cos(phi),1]);
 a=conv(a,[1,-2*r*cos(phi),r^2]);
end

Te=-filter([1,-1],1,...
    unwrap(angle(freqz(b,a,2*pi*fopt*Ts)))./ ...
    filter([1,-1],1,(2*pi*fopt));
Tcmp=Tdpopt+Te;
Err=(max(Tcmp)-min(Tcmp))

for i=1:order/2
 G(i)=x(2*i-1)-0.99;
 G(i+order/2)=-x(2*i-1);
end
```

REFERENCES

1 Tlusty, J., 1985, "Machine Dynamics," Handbook of High Speed Machining Technology, Editor, R. I. King, Chapman and Hall, New York, pp. 49-153.

2 Tlusty, J., Smith, S., Badrawy, S. J., Smith, D. A., Smith, A. P., 1997, "Design of High Speed Milling Machine for Aluminum Aircraft Parts," ASME MEC Vol. 6-2, pp. 323-332.

3 United States General Accounting Office, 1997, Acquisition Reform Effect on Weapon System Funding, GAO/NSIAD-98-31.

4 Kandebo, S. W., 1995, "V-22 Modifications Focus on Cost, Producibility," Aviation Week and Space Technology, Vol. 142, No. 21, pp. 35-38.

5 Koren, Y., Lo, C. C., 1992, "Advanced Controllers for Feed Drives," Annals of the CIRP, Vol. 41/2, pp. 689-698.

6 Alter, D. M., Tsao, T. C., 1996, "Control of Linear Motors for Machine Tool Feed Drives: Design and Implementation of H_∞ Optimal Feedback Control," Transactions of the ASME, Journal of Dynamic Systems, Measurement and Control, Vol. 118, pp. 649-656.

7 Van Brussel, H., Van den Braembussche, P., 1998, "Robust Control of Feed Drives with Linear Motors," Annals of CIRP, Vol. 47/1, pp. 325-328.

8 Koren, Y., 1980, "Cross-Coupled Biaxial Computer Control for Manufacturing Systems," Transactions of the ASME, Journal of Dynamic Systems, Measurement, and Control, Vol. 102, pp. 265-272.

9 Tomizuka, M., 1987, "Zero Phase Error Tracking Algorithm for Digital Control," Transactions of the ASME, Journal of Dynamic Systems, Measurement, and Control, Vol. 109, pp. 65-68.

10 Tomizuka, M., 1987, "Adaptive Zero Phase Error Tracking Algorithm for Digital Control," Transactions of the ASME, Journal of Dynamic Systems, Measurement, and Control, Vol. 109, pp. 349-354.

11 Weck, M., Ye, G., 1990, "Sharp Corner Tracking Using the IKF Control Strategy," Annals of the CIRP, Vol. 39/1, pp. 437-441.

12 Chen, Y., Tlusty, J., 1995, "Effect of Low-Friction Guideways and Lead-Screw Flexibility on Dynamics of High Speed Machines," Annals of CIRP, Vol. 44/1, pp. 353-357.

13 Przemieniecki, J. S., 1968, Theory of Matrix Structural Analysis, Dover Publications, New York.

14 Franklin, G. F., Powell, J. D., Workman, M. L., 1990, Digital Control of Dynamic Systems, Addison-Wesley, Reading, MA.

15 Oppenheim, A. V., Schafer, R. W., 1989, Discrete-Time Signal Processing, Prentice Hall, Englewood Cliffs, NJ.

16 Deczky, A. G., 1979, "Program for Minimum -p Synthesis of Recursive Digital Filters," Programs for Digital Signal Processing, IEEE Press, New York, Sect. 6.2, pp. 1-38.

BIOGRAPHICAL SKETCH

David Alan Smith was born on May 4, 1965, in Pittsburg, Kansas. He grew up in the beautiful city of Tallahassee, Florida, where he successfully completed the grades of kindergarten through twelve without repetition. He then spent two unmotivated years at Tallahassee Community College. After transferring to Florida State University, without much science or mathematics background, he decided to study engineering. He made that decision because he needed to declare a major and it seemed that would be a sensible career choice. Sometime during the middle of a semester of Physics I and Calculus II he discovered a fascination with his studies and has been hooked on understanding the physical world ever since.

He then moved to Gainesville, Florida, to attend the University of Florida to study mechanical engineering. He received a Bachelor of Science degree in mechanical engineering in 1989. After graduation, he worked briefly in the petrochemical industry before returning to the University of Florida to begin work toward a Master of Science degree. While working on his master's research project, in the Machine Tool Research Center, he discovered a wonderful satisfaction from successfully applying theoretical knowledge to practical engineering problems. He then realized he had "lucked" into the right career.

After earning a Ph.D. degree, the author plans to practice engineering outside of the academic setting. He will also pursue many old and new interests with his lovely wife Donna.

I certify that I have read this study and that in my opinion it conforms to acceptable standards of scholarly presentation and is fully adequate, in scope and quality, as a dissertation for the degree of Doctor of Philosophy.

Jiri Tlusty, Chairman
Graduate Research Professor of
Mechanical Engineering

I certify that I have read this study and that in my opinion it conforms to acceptable standards of scholarly presentation and is fully adequate, in scope and quality, as a dissertation for the degree of Doctor of Philosophy.

John C. Ziegert
Associate Professor of Mechanical
Engineering

I certify that I have read this study and that in my opinion it conforms to acceptable standards of scholarly presentation and is fully adequate, in scope and quality, as a dissertation for the degree of Doctor of Philosophy.

John K. Schueller
Associate Professor of Mechanical
Engineering

I certify that I have read this study and that in my opinion it conforms to acceptable standards of scholarly presentation and is fully adequate, in scope and quality, as a dissertation for the degree of Doctor of Philosophy.

Gloria J. Wiens
Associate Professor of Mechanical
Engineering

I certify that I have read this study and that in my opinion it conforms to acceptable standards of scholarly presentation and is fully adequate, in scope and quality, as a dissertation for the degree of Doctor of Philosophy.

Jacob Hammer
Professor of Electrical and Computer Engineering

This dissertation was submitted to the Graduate Faculty of the College of Engineering and to the Graduate School and was accepted as partial fulfillment of the requirements for the degree of Doctor of Philosophy.

August 1999

M. J. Ohanian
Dean, College of Engineering

Winfred M. Phillips
Dean, Graduate School